Wave Forces on Transition Pieces for Bucket Foundations for Offshore Wind Turbines

Nezhentseva, Anastasia; Andersen, Thomas Lykke; Andersen, Lars Vabbersgaard; Ibsen, Lars Bo

Publication date:
2012

Document Version
Publisher's PDF, also known as Version of record

Wave Forces on Transition Pieces for Bucket Foundations for Offshore Wind Turbines

Anastasia Nezhentseva
Thomas Lykke Andersen
Lars V. Andersen
Lars Bo Ibsen

ISSN 1901-7278
DCE Technical Memorandum No. 28

AALBORG UNIVERSITY
Department of Civil Engineering

Aalborg University
Department of Civil Engineering
Division for Structures, Materials and Geotechnics

DCE Technical Memorandum No. 28

Wave Forces on Transition Pieces for Bucket Foundations for Offshore Wind Turbines

by

Anastasia Nezhentseva
Thomas Lykke Andersen
Lars V. Andersen
Lars Bo Ibsen

November 2012

Scientific Publications at the Department of Civil Engineering

Technical Reports are published for timely dissemination of research results and scientific work carried out at the Department of Civil Engineering (DCE) at Aalborg University. This medium allows publication of more detailed explanations and results than typically allowed in scientific journals.

Technical Memoranda are produced to enable the preliminary dissemination of scientific work by the personnel of the DCE where such release is deemed to be appropriate. Documents of this kind may be incomplete or temporary versions of papers—or part of continuing work. This should be kept in mind when references are given to publications of this kind.

Contract Reports are produced to report scientific work carried out under contract. Publications of this kind contain confidential matter and are reserved for the sponsors and the DCE. Therefore, Contract Reports are generally not available for public circulation.

Lecture Notes contain material produced by the lecturers at the DCE for educational purposes. This may be scientific notes, lecture books, example problems or manuals for laboratory work, or computer programs developed at the DCE.

Theses are monograms or collections of papers published to report the scientific work carried out at the DCE to obtain a degree as either PhD or Doctor of Technology. The thesis is publicly available after the defence of the degree.

Latest News is published to enable rapid communication of information about scientific work carried out at the DCE. This includes the status of research projects, developments in the laboratories, information about collaborative work and recent research results.

Published 2012 by
Aalborg University
Department of Civil Engineering
Sohngaardsholmsvej 57,
DK-9000 Aalborg, Denmark

Printed in Aalborg at Aalborg University

ISSN 1901-7278
DCE Technical Memorandum No. 28

Wave Forces on Transition Pieces for Bucket Foundations for Offshore Wind Turbines

Anastasia Nezhentseva, Thomas Lykke Andersen, Lars Vabbersgaard Andersen and Lars Bo Ibsen
Aalborg University, Department of Civil Engineering, Sohngaardsholmsvej 57, Aalborg, 9000, Denmark,
E-mails: an@civil.aau.dk, tla@civil.aau.dk, la@civil.aau.dk, lbi@civil.aau.dk

ABSTRACT

Since offshore wind turbines continually increase in size and move to deep water depths (>25 m), significant wave loading becomes a major concern for their design. A monopile foundation is one of the most commonly used types of the offshore wind turbine foundations today. This solution, however, becomes not very cost-effective in deep water depths. Therefore, it is essential to find some alternative economically efficient solutions. This paper presents an experimental study of wave loading on several shapes of transition pieces (TPs) used to transfer the loads from a 5 MW offshore wind turbine to a bucket foundation (suction caisson) located at 35 m water depth in the North Sea. Several models of the TPs (wedge-shaped steel flange-reinforced shear panels, conical and doubly curved with or without cutaways) are tested in a wave flume and compared with respect to wave loading. Due to a larger size of the suggested TPs compared to a typical slender monopole foundation, wave loads acting on these TPs are also expected to be considerably higher and much more difficult to predict. The results of the present investigation can be further applied for other wind turbine types.

Keywords:
Offshore wind turbine, transition piece, bucket foundation, wave loads.

1. Introduction

The bucket foundation (suction caisson) is a well-known concept from the oil and gas industry, where it has been used for more than 30 years for oil platforms installed in the North Sea. Recently, this concept has been introduced in the offshore wind industry as an environmentally-friendly alternative to other types of wind turbine foundations. However, when implementing the bucket foundation concept to offshore wind turbines, special consideration must be given to loading conditions which are significantly different from jacket structures used within the oil and gas sector. Thus, offshore structures in the oil and gas industry are typically multi-legged structures acting mainly in compression−tension (so-called “push−pull” action). On the contrary, for offshore wind turbines on suction bucket monopods or caisson-based multipods, the resulting horizontal loading

from wind and waves can be 50−150% of the vertical loading, thus creating large overturning moments on bucket foundations.

Moreover, installation of a bucket foundation requires only a small vessel floating it on site. Penetration the foundation into the seabed is partially performed by its self-weight and partially by suction created by a pump used to evacuate the water inside the bucket. A water flow is generated in the subsoil as a side effect of the reduced pressure inside the bucket, which leads to a reduction of the effective stresses near the tip of the skirt, consequently resulting in easier penetration. The suction pump is the only source of underwater sound emission, which is not comparable to a high-noise impact of hydraulic hammers and drill drives used, for example, for installation of monopile foundations. Therefore, this installation technique does not produce underwater noise of impulsive nature which can potentially be harmful for marine mammals, making it advantageous compared to other types of offshore wind turbine foundations. Another benefit of the bucket foundation is its possibility of reuse and recycling if a wind farm is to be decommissioned at the end of service life. In this case, the bucket can be lifted out from the seabed by reversing the suction procedure by means of applying water pressure into the bucket skirt.

In countries like Denmark and the UK wind farms are being planned at 35−55 m water depth in the North Sea, primarily due to the lack of offshore areas with smaller water depths. This, in return, might create additional loading on offshore wind turbine structures due to waves and current. As a result, application of the monopile foundation becomes limited as its stiffness is considerably smaller compared to other foundation solutions for deeper waters. Consequently, additional research on hydrodynamic loading on substructures of wind turbines is required.

The present research focuses on such loading of a transition piece (TP), here defined as a structural element positioned between the wind turbine tower and the bucket foundation. Currently, wedge-shaped steel flange-reinforced stiffeners connected to the lower part of the tower and radially positioned on top of the bucket lid are used as TPs for bucket foundations. However, production and installation of these stiffeners is time-consuming and expensive, since extensive welding followed by reliable corrosion protection is required. Besides, repeated wave and wind action can cause fatigue at the welded joints and, consequently, deterioration of steel over time. Thereby, finding an additional solution for the TP production without compromising its stiffness and strength, along with avoiding significant increase in wave loads and keeping the manufacturing costs low would be a desired outcome of the present study.

Nezhentseva et al. [1,2] proposed Compact Reinforced Composite (CRC) as an alternative to steel for the production of a TP. CRC is a high performance steel-fibre reinforced concrete developed at Aalborg Portland A/S, Denmark. It normally contains 2−6% by volume of 0.16×6 mm or 0.4×12.5 mm steel fibres. Research carried out by Nezhentseva et al. [1,2] resulted in the

proposal of several shapes of the TPs for future investigation with respect to hydrodynamic loading as well as potential threat of seabed scour. Due to the complexity of the geometry of the proposed shapes of the TPs, determination of wave loads is complicated.

This paper presents results from small-scale tests in which the wave forces on transition pieces with different shapes and intended for use at water depths of about 35 m have been found. The motivation for the experiments is to obtain a description of wave forces acting on various forms of TPs as the hydrodynamic loading on the TP itself is part of the design loop with respect to its load bearing capacity. Furthermore, for such structures compared to a monopile there are much higher uncertainties on the load coefficients, and shielding effects can occur.

The present paper is organised as follows: Section 2 presents state of the art, Section 3 describes hydrodynamic loading, wave theories, scaling law used in the small-scale tests, load models and load coefficients, Section 4 covers the experimental setup, Section 5 reviews methodology, Section 6 presents the results, main findings, discussion and modelling inaccuracy and, finally, Section 7 summarizes the conclusions.

2. Literature review

Currently, physical hydraulic model tests (small-scale or prototype) and various numerical computational models simulating wave forces and wave run-up phenomena are used for prediction and evaluation of hydrodynamic loading on offshore wind turbine structures. Computational Fluid Dynamics (CFD) modelling based on the Navier−Stokes equations has become widely used within recent years for analysis of the flow problems for offshore wind turbine foundations and is often considered an alternative to physical laboratory tests. Different programs and codes exist that are able to provide an insight into the physics of the hydrodynamic problem. For example, DHI in Denmark developed the CFD code NS3 based on a three-dimensional (3D) Navier−Stokes solver. Description and validation of the method can be found in Mayer et al.[3], Emarat et al. [4], Nielsen and Mayer [5], Christensen [6], Bredmose et al. [7] (reproduction of extreme wave loads on a gravity wind turbine foundation), and Christensen et al. [8] (wave forces and wave run-up). Wave−current interaction is not taken into account in the present study but should normally be investigated for deeper water depths where current action becomes significant. For example, Li et al. [9] carried out physical model experiments on the in-line and lift forces on vertical piles induced by irregular waves combined with currents. Lately, Markus et al. [10] developed a numerical wave channel for realistic offshore conditions for gravity base foundations subjected to wave−current interaction. This wave channel utilized the CFD software package OpenFOAM based on the solution of the unsteady Reynolds-averaged Navier−Stokes (RANS) equations combined with a

non-linear wave model (two equation turbulence model) and the Volume-of-Fluid method to simulate an unsteady sea state.

Wave induced forces on cylinder members were investigated extensively over the last several decades by, among others: Sarpkaya [11], Sarpkaya and Isaacson [12], and Chakrabarti [13,14]. Experimental studies were carried out on wave loading on a slender cylindrical pile in shallow waters, see, i.e. Peeringa [15], Larsen and Frigaard [16]. By means of large-scale laboratory tests, Mo et al. [17] validated the results obtained with a 3D numerical model of non-breaking wave forces on slender piles based on Euler's equations. Moreover, a 3D numerical wave basin model developed using the multi-physics finite-element based nonlinear numerical code LS-DYNA, containing both fluid and structural models, was used by Zhang [18] to evaluate results of experiments on tsunami solitary wave impact on a vertical cylinder. Detailed investigation of the vertical distribution of the wave forces on circular cylinders was performed by Høgedal [19]. Breaking and wave slamming loads acting on a monopile as well as wave run-up phenomenon have been studied, among others, by Wienke et al. [20], de Vos et al. [21], Christensen et al. [8] and Lykke Andersen et al. [22].

Moreover, Lykke Andersen and Frigaard [23] performed a set of prototype large-scale tests on a concrete cone and monopile foundations in 9−15 m water depth. Besides, Modridge and Jamieson [24] experimentally measured wave forces and overturning moments on large vertical caissons of square shape oriented either with one side perpendicular to the direction of wave propagation or with the sides rotated 45º relative to the wave propagation direction. They confirmed the obtained results using an approximate theoretical method based on the diffraction theory of MacCamy and Fuchs [25]. Furthermore, Au and Brebbia [26] applied the boundary element method (BEM) for computing wave forces on cylindrical offshore structures of circular, square and elliptical shape and compared the solutions against analytical or experimental results. Numerical calculations of forces induced by short-crested waves on vertical cylinders of circular, elliptical and square cross-sections using the BEM were also performed by Zhu and Moule [27]. In their work they investigated short-crested waves, known to represent waves generated by winds in the ocean more accurately, but diffracting and reflecting in a more complex manner than plane waves. A comparison was made with plane waves with the same total wave number, finding that the wave loads induced by short-crested waves produce larger wave forces on a cylinder of non-circular cross-section. General lack of research, however, exists in the area of assessment of hydrodynamic loading on various types of offshore wind turbine foundations, i.e. 3− or 4−legged jackets, bucket foundations with different transition pieces and gravity foundations located in deep waters.

3. Hydrodynamic Loading

Differences in wave kinematics might cause variations in the results of the experiments on hydrodynamic loading. Generally, wave load experiments can be used for validation of numerical wave load models, as well as for estimation of the load coefficients for inertia and drag in the Morison equation. Furthermore, undisturbed wave kinematics, which is used as an input for the Morison equation, can be measured in the wave flume at the location of the model without the structure itself. Finally, wave loads acting on the model can be calculated using a carefully selected wave theory and a proper load model and compared with the laboratory wave load measurements.

3.1. Wave theories

Several wave theories representing the kinematics of hydrodynamic loading can be applied for calculation of wave loads. The choice of a suitable wave theory can be made based on the range of its validity, water depth and type of waves, i.e. breaking, non-breaking, post-breaking. Several analytical or numerical wave theories are used to represent the kinematics of regular waves. According to the Offshore Standard DNV-OS-J101 [31] the following theories are used for characterizing hydrodynamic loading: for small-amplitude deep water waves − Linear wave theory (or Airy theory, [32]) with a sinusoidal wave profile; for high waves − Stokes wave theories [33]; for shallow water waves − Boussinesq higher-order theory and Solitary wave theory. Moreover, stream function theory based on numerical methods where nonlinear equations can be simultaneously solved was introduced by Dean [34]. This theory precisely represents the wave kinematics and can be used for a wide range of water depths. Moreover, according to among others LeMehaute et al. [35] and Dean [36], stream function theory has a better fit to measured laboratory wave data compared to the results from Stokes wave theory known to break down in shallow waters (see, e.g. Fenton [37]).

Normally, for the given wave parameters wave kinematics can be calculated using a relevant wave theory. Linear wave theory (LWT) is known to be the least complicated theory, but it is, however, limited to the design of non-breaking waves with small wave height, H, compared to the wavelength, L, and water depth, h, i.e. small values of H/L and H/h. In reality, waves are not regular sine-shaped monochromatic waves and, therefore, LWT can lead to unsafe design. Stream function and linear wave (Airy or Stokes 1st order) theories can predict well the kinematics for non-breaking waves and underestimate it for breaking and post-breaking waves, thus becoming insufficient for further estimation of the wave loads.

Nonlinear wave theories (the Stokes 5th order theory or stream function theory) are currently used in case regular waves are used for ULS design of the offshore structures and are best

suitable for waves in deeper water. Moreover, Fenton [37] developed a fifth-order cnoidal wave theory for waves in shallower water and compared its numerical results with experimental measurements. According to his findings, the high-order cnoidal wave theory gives quite accurate results for wavelengths greater than eight times the water depth and should be used as an alternative to fifth-order Stokes wave theory. Furthermore, stream function theory can be applied to non-linear theoretical wave and can be employed to represent wave conditions with uniform steady current. The form of a stream function is selected in such a way that it is a solution to Laplace's equation. Stream function theory is a more accurate method compared to linear wave theory, especially in case if the wave height is greater than 50% of the breaking height (see, e.g. Dean [34]). The higher order wave theories take into consideration the influence of the wave itself on its characteristics (wave length, phase velocity, shape of the surface).

3.2. Load Models

Wave load prediction theories should properly take into account the type, shape and size of the TP for an offshore wind turbine. The Morison equation (see Morison et al. [38]) is normally applied to calculate the wave loads for slender structures, such as jacket structure components and monopiles according to DNV-OS-J101 [31]. The Morison load formula is a sum of an inertia force proportional to acceleration and a drag force proportional to the square of velocity. In addition, the Morison equation only takes into account horizontal loads, but when the TP has oblique or doubly curved surfaces as suggested in the previous study [1,2], the dynamic pressure from the water acts perpendicular to the inclined surfaces of the foundation; see Figure 1 showing the dynamic pressure distribution from the wave loading around a monopile (Figure 1a) and two shapes of the TPs on the bucket foundations (Figure 1b and 1c) installed in deep water depths (> 35 m). Each side of the foundation experiences time-varying wave forces from fluctuating dynamic wave pressures differing on the up-wave and down-wave sides. Under the wave crest (up-wave direction) the dynamic wave pressure is positive, and it applies compression on a foundation, shown on the left of the substructures. Under the trough (down-wave direction) the dynamic pressure is negative, and there is a drag (suction) on the right side of the foundations.

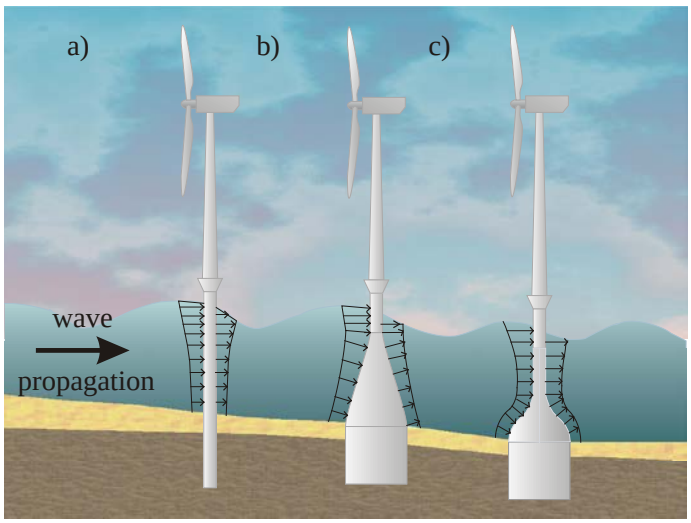

Figure 1: A sketch of the maximum inertia pressure distribution around different types of foundations for offshore wind turbines: a) monopile; b) suction bucket with conical shell transition piece. c) suction bucket with doubly curved shell transition piece.

It is assumed in the Morison equation that the liquid particles follow a path, where an individual particle moves around the foundation at the same level. In reality, fluid particles will move towards minimum drag and, therefore, have a trajectory such as the particles pass the TP in the area of its smallest diameter. This will affect the loading of the TP, as the attack points of the wave forces will become too low compared to reality. On the other hand, moment contributions from the pressure components that act perpendicular to the inclined surfaces will lead to the reduction of the moments. These two effects will work against each other. Therefore, for a bucket foundation with a traditional TP connected directly to the wind tower (resembling a monopile), the moment reduction could be expected; while for the other two forms (Figure 1b-1c) an increase of the moment contributions is anticipated.

Wave diffraction analysis, however, shall be carried out to investigate local (pressure force) and global wave loads for large volume structures, e.g. gravity foundations. For these types of offshore structures the wave kinematics is expected to be disturbed by the presence of the structure. When the diameter of the TP becomes larger than 1/5 of the wavelength, the Morison equation will be no longer valid as diffraction and reflection of the waves should be taken into consideration. Inertia term for such cases can be calculated using the MacCamy-Fuchs solution [25] in combination with the drag force calculated according to the Morison equation (see, e.g. DNV-OS-J101 [31]) or using various numerical calculation programs. The Morison equation, where the MacCamy-Fuchs solution is used for calculation of the inertia term, applies, however, only for circular cylinders and can, thereby, be only an approximate solution for TPs with a varying

diameter over depth. Wave forces acting on such structures with inclined surface areas can be calculated by subdividing the overall height into small sub-elements of the height Δh, where the wave forces are assumed to attack at the centre of each sub-element. For each sub-element, Simpson integration can be performed and the related moment reaction at the seabed can be found. The resultant force will be a sum of the wave forces acting on all the elements and the corresponding attack point can be found by dividing the resultant moment reaction by the resultant wave force. More advanced models, such as Boussinesq wave model (see, e.g. Madsen [39]) and the wave impact load model of Wienke [40], are suggested to be used if breaking waves becomes an issue.

3.3. Scaling

According to the Offshore Standard [31], hydrodynamic model tests or full scale measurements should be carried out to support theoretical predictions subjected to significant uncertainties. These tests are supposed to verify the above mentioned available analytical methods, to support theoretical calculations when the wave load prediction theory is prone to large uncertainties, and to check that important hydrodynamic features have not been disregarded by altering the wave parameters. Yet, in order to make a reliable analysis of the full-scale measurements, sufficient instrumentation, costly facilities and environmental conditions recording is normally required. In contrast, small-scale tests are inexpensive and faster to perform to study hydrodynamic loading phenomenon and to make a comparison of the wave loads on various shapes of the TPs in a controlled manner. Small-scale tests, however, can induce some uncertainties related to scale effects. Reliable results can be expected from small-scale tests if the scale effects are insignificant which will be the case if the inertia loads are dominating and Froude scaling is applied. In these tests the length-scale factor (Froude) is $\alpha_L = 1{:}100$. Furthermore, the characteristic Reynolds number in the models experiments is normally less than its critical value for which the drag coefficient has the smallest value. This will lead to the values of the wave loads to be on the unsafe side. If the drag is significant, the model results will usually be conservative.

Normally models tested in the scale-model testing have a smooth surface, whereas the surface of the prototype models installed offshore can be initially smooth but become rough over time due to marine growth development. Besides, marine growth increases the cross-sectional dimensions of the substructure below the water table. Hence, the volume and the mass of the TP structure will also increase. The combination of these factors will consequently lead to increase of the wave forces acting on the TP structure. Therefore, it is important to choose a proper drag coefficient for the wave load calculations on the prototype using the Morison equation and increase

the model dimensions by accounting marine growth based on recommendations from standards, e.g. DNV-RP-C205 [41].

3.4. Load Coefficients

The drag (C_D) and the inertia (or mass) (C_M) coefficients used in the Morison´s load formula depend mainly on the Keulegan-Carpenter number $KC = \frac{V_m \cdot T}{D}$, the Reynolds number $Re = \frac{V \cdot D}{\nu}$ and the roughness $\Delta = \frac{k}{D}$ (DNV- RP-C205 [41]). For prototype conditions, the Reynolds number is so large that fully turbulent flow exists and, thus, the load coefficients become independent of Re. The following wave characteristics have been reported for a 50 year return period and 35 m water depth at several locations in the North Sea along the British coast by a met ocean design data report from a reliable source in the Danish energy sector [42]: maximum wave height H_{max} = 14−16.2 m, significant wave height H_s = 7.5−9.4 m and peak wave period T_p = 10.3−14.2 s. Høgedal [19] refers to a natural extreme situation for a prototype with H_s = 11 m and T_p = 16 s. Plunging breaking waves are not likely to be observed in-situ according to the Danish report [43] and Peeringa [15], stating that wave breaking is insignificant in the North Sea for water depths greater than 20 m. Therefore, for a monopile prototype placed in the North Sea in a natural extreme situation (D = 7.5 m; h = 35 m and t = 10ºC) with highly irregular waves generated by a storm with significant wave heights H_s = 7.5−11 m and peak periods T_p = 10.3−16 s, the following variations will be expected for the design wave: $9 < KC < 27$ and $5 \cdot 10^7 < Re < 1 \cdot 10^8$. As for the laboratory experiments, the Reynolds number Re is $100^{1.5}$ = 1000 times smaller disregarding any differences in viscosity.

According to DNV-OS-J101 [31] for 30 to 40 m water depths in the southern and central parts of the North Sea, C_D = 0.8 and C_M = 1.6 for prototype conditions with high Re ($Re > 10^6$). Surface roughness depends on the material used for the production of the TP structures, whether the surface is newly coated or corroded, and on the presence of marine growth which will increase the cross-sectional dimensions of the TPs (see, i.e. DNV-RP-C205 [41]**).** The effect of marine growth should also be considered when selecting drag coefficients. Consequently, for $Re > 10^6$ and large KC numbers (KC > 20−50) when the drag force is dominating compared with the inertia force, C_D = 1.05 and the asymptotic value for the added mass coefficient C_A = 0.2 ($C_M = 1 + C_A$ = 1.2) for rough cylinders ($\Delta > 10^{-2}$), respectively (DNV-RP-C205 [41]). As a result, for a prototype located at 35 m water depth with supercritical Re and rough surface of the structures the expected values of the C_M and C_D coefficients will be in the range of C_M = 1.2 – 1.6 and C_D = 0.8 −1.05.

As for the model conditions with lower Re and smooth surface of the structures, for $KC < 3$ the expected mass coefficient will be C_M = 2.0, while for larger KC numbers the added mass coefficient will be C_M = 1.6 (DNV-RP-C205 [41]). As for the drag coefficient, for KC > 20−50, Re

$> 10^6$ and $\Delta < 10^{-4}$ $C_D = 0.65$ (DNV-RP-C205 [41]). These values are in good agreement with the results for the drag coefficient $C_D \approx 0.65-0.7$ for the smooth model cylinder obtained by Sarpkaya and Isaacson [12] for KC = 20-30 and $Re = 1 \cdot 10^5$.

4. Experimental setup

Laboratory experiments were carried out in a wave flume at Aalborg University, Denmark. The layout of the basin is shown in Figure 2. The flume was 1.2 m wide, 18.65 m long and up to 1.5 m deep. A sloping stone layer (absorption beach) was used in the end opposite to the wave generator to absorb the main part of the incident energy from waves and to reduce their reflection. The bottom of the wave flume was horizontal in the middle, where the model was placed, followed by slopes towards the absorption beach and the wave generator. The water depth at the model was 0.35 m while the water level at the wave maker was 0.75 m.

The surface elevations were measured with three resistance-type wave gauges in order to isolate the incoming and reflected waves. The middle wave gauge was located 1.9 m in front of the centre of the model (see Figure 2). The wave loads acting on the monopile and various shapes of the TPs were transferred to a force transducer connected to the top of the models. The force transducer had strain gauge full bridges placed at two sections. The transducer was calibrated in such a way that the output voltage could be transformed into moments at these two sections which were further converted to force and corresponding attack point. There was a small gap between the bottom of each TP model and the wave flume, which was done in order to make sure that all the wave loads had been transferred to the force transducer. If forces acting on the TPs, on the contrary, were to be delivered to the bottom of the flume, the wave loads could not have been measured. On the other hand, placing the models above the seabed level might have provided a model error, since it caused a flow below the TPs. The transducer was chosen so stiff that no significant dynamic amplification of the loads occurs for non-breaking waves.

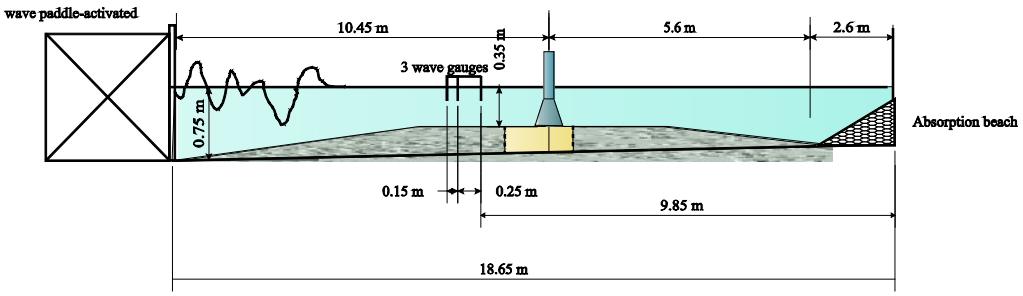

Figure 2. Layout of the wave flume for wave force measurement.

5. Methodology

Two loading situations are considered with the incoming regular and irregular waves. Comparison of the experimental measurements is performed for a reference case (monopile) to the calculated load estimations using different wave theories. The desired outcome of the wave experiments will be finding a shape of the TP with a better performance in a deep water wave environment, studying the effect of cutaways on the wave loading as well as further recommendations for the design of the TPs on the bucket foundations.

Eight models were suggested for the experimental study of wave loading on various shapes of the TPs on bucket foundations. The diameter of the tower used for the experiments was 7.5 cm, the bucket foundation diameter was 20 cm. The description of the laboratory models is given in Table 1 and the models are shown in Figure 3.

The choice of the models was based on the structural optimization performed in the earlier research work done by Nezhentseva et al. [1,2,28]. The same TP models were tested for scour development and the results were presented earlier [28]. A smooth cylinder with diameter D = 0.075 m was chosen as a reference case reproducing a monopile foundation. Model TP2 characterizes the current solution used in the design of the TPs for bucket foundations suggested by Universal Foundation A/S, Aalborg, Denmark.

Model TP3 was chosen earlier as the one providing a smooth force transition from the wind turbine tower to the bucket foundation at the convex and concave parts [2]. Conical shape models TP5-TP7 were also shown to provide a uniform force distribution from the tower to the bucket skirt [1]. Initially, a decision regarding removing part of the material and creating several cutaways was made with the intention of saving some material (CRC) and minimizing potential scour (see Nezhentseva et al.[2,28]). In this research cutaways were further examined for potential reduction of wave forces acting on the substructures. From a structural point of view model TP6 with large oval holes is prone to buckling which might occur under concentrated loads due to bearing compressive stresses from self-weight of the wind turbine tower combined with wind and wave loading. Hence, structural design of the model TP7 took into consideration instability risk by having additional horizontal stiffeners providing extra stability to the TP structure. The final conical model (TP8) − a 6-legged TP structure with hollow circular columns made of CRC − had six round streamlined members.

Table 1. Laboratory scale models description

Acronym	Description of the model
	Monopile (D = 0.075 m)
TP2	Traditional TP with ribs, flanges and holes in ribs (steel)
TP3	Doubly curved solid TP (CRC)
TP4	As TP3 but with 3×8=24 circular hole array with different diameters through the height (CRC)
TP5	Truncated conical solid TP (CRC)
TP6	As TP5 but with 6 oval holes (CRC)
TP7	As TP5 but with 3×6=18 trapezoidal hole array (CRC)
TP8	TP with six round-shaped legs (CRC)

Model TP8 was chosen for investigation and comparison of the effect of the streamlined elements (columns) and the sharp edges of simple cutaways implemented in models TP4, TP6 and TP7 on the wave forces. Cutaways and streamlined elements would be expected to reduce the wave forces acting on the substructures. Furthermore, in case of achievement of the reduction of the wave forces acting on the TPs, optimization of the cutaways can be expected to be performed not only according to structural performance, but also according to wave loading.

During the experiments the cutaways of the models TP6 and TP7 were oriented with respect to wave direction as shown in Figure 4. TP6 was oriented with its oval cutaway towards the upcoming wave, whereas TP7 faced the waves with a solid part with three trapezoidal holes symmetrically placed to both of its sides. Although orientation of the cutaways might have some influence on the wave forces, it has not been studied in the present work.

The natural frequency and damping ratio in water, i.e. including added mass, was measured by applying an initial movement to the models and are summarized in Table 2. In order to minimize the influence of the high frequency noise, the data of the wave tests was filtered by a digital filter with a cut-off frequency of 5 Hz. A digital filter was also applied to remove dynamic amplification and, thus, convert loads to an infinite stiff structure. The sampling frequency was chosen to 20 Hz.

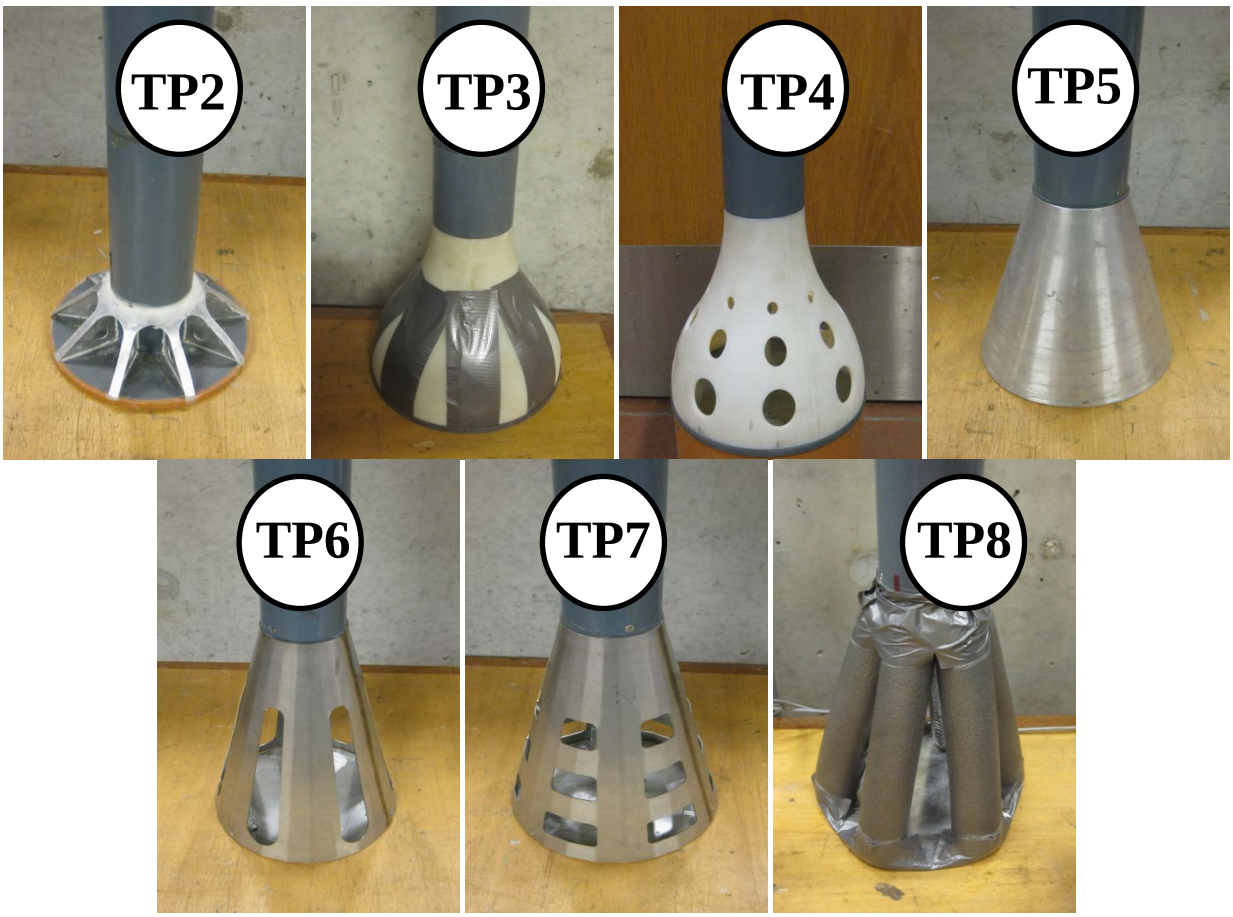

Figure 3. Laboratory scale models of the transition pieces on bucket foundations

Table 2 Eigen frequencies and damping ratios for the TP models

Model	Monopile	TP2	TP3	TP4	TP5	TP6	TP7	TP8
Eigen Frequency [Hz]	4.416	3.757	2.623	3.57	2.502	3.927	3.789	3.387
Damping Ration	0.024	0.054	0.017	0.040	0.045	0.057	0.063	0.049

Figure 4. Positioning of the models TP6 (to the left) and TP7 (to the right) regarding the waves during the experiments.

5.1. Regular waves

Regular waves of varying height were generated in the laboratory experiments by second order control signal in accordance with Schäffer [43]. All tests with regular waves were conducted with a water depth of h = 0.35 m, a wave period of T = 1.4 s and assigned wave heights of H = 0.02−0.24 m with a step of 0.02 m (corresponding to 35 m, 14 s and 2−24 m, respectively, in prototype scale). Twelve tests were performed on each model for a duration of 1 minute. The water depth to wavelength ratio in the experiments was h/L = 0.14, which corresponds to intermediate depth. The regular wave loads within the reference case, i.e. the monopile, were directly compared to the calculated Morison forces, determined using kinematics of the linear and stream function wave theories. It was observed during the experiments that the generated waves were close to regular over the duration of one test.

5.2. Irregular waves

In real sea conditions, there are no periodic regular waves, only irregular waves. Therefore, irregular waves were generated in the experiments in order to obtain a more realistic presentation of the sea state. Breaking waves were not observed during the experiments. Irregular waves were generated using linear theory and a JONSWAP spectrum defined according to ISO19901 [44] with a peak enhancement factor 3.3 with two assigned significant wave heights of H_s = 0.095 and 0.115 m and a peak period T_p = 1.4 s (equivalent to 9.5; 11.5 m and 14 s in prototype conditions). During each test 1000 irregular waves were generated.

6. Results and discussion

6.1. Regular waves

Average maximum peak forces and moments are plotted against wave heights for various TP models in Figures 5 and 6 and are compared to the experimental results for the reference case (monopile). For the monopile, the calculated loads using the Morison equation and stream function wave theory (SFWT) and linear wave theory (LWT) are also included. The load coefficients were taken as best fit constant values being C_D = 1.5; C_M = 2 and C_D = 0.8; C_M = 2 for LWT and SFWT, respectively, which for SFWT are in agreement with the expected values from Section 5. Using these coefficients the horizontal maximum forces and moments are generally in good agreement with the calculated values, however with some scatter, especially for the moments resulting from the higher waves (Figure 6a).This might be due to the fact that the Morison equation provides a simple estimate of the loads on the monopile. Moreover, possible deviation between the experimental results and the theory could be due to the drag coefficient C_D varying with Re and, thus, wave height and surface elevation.

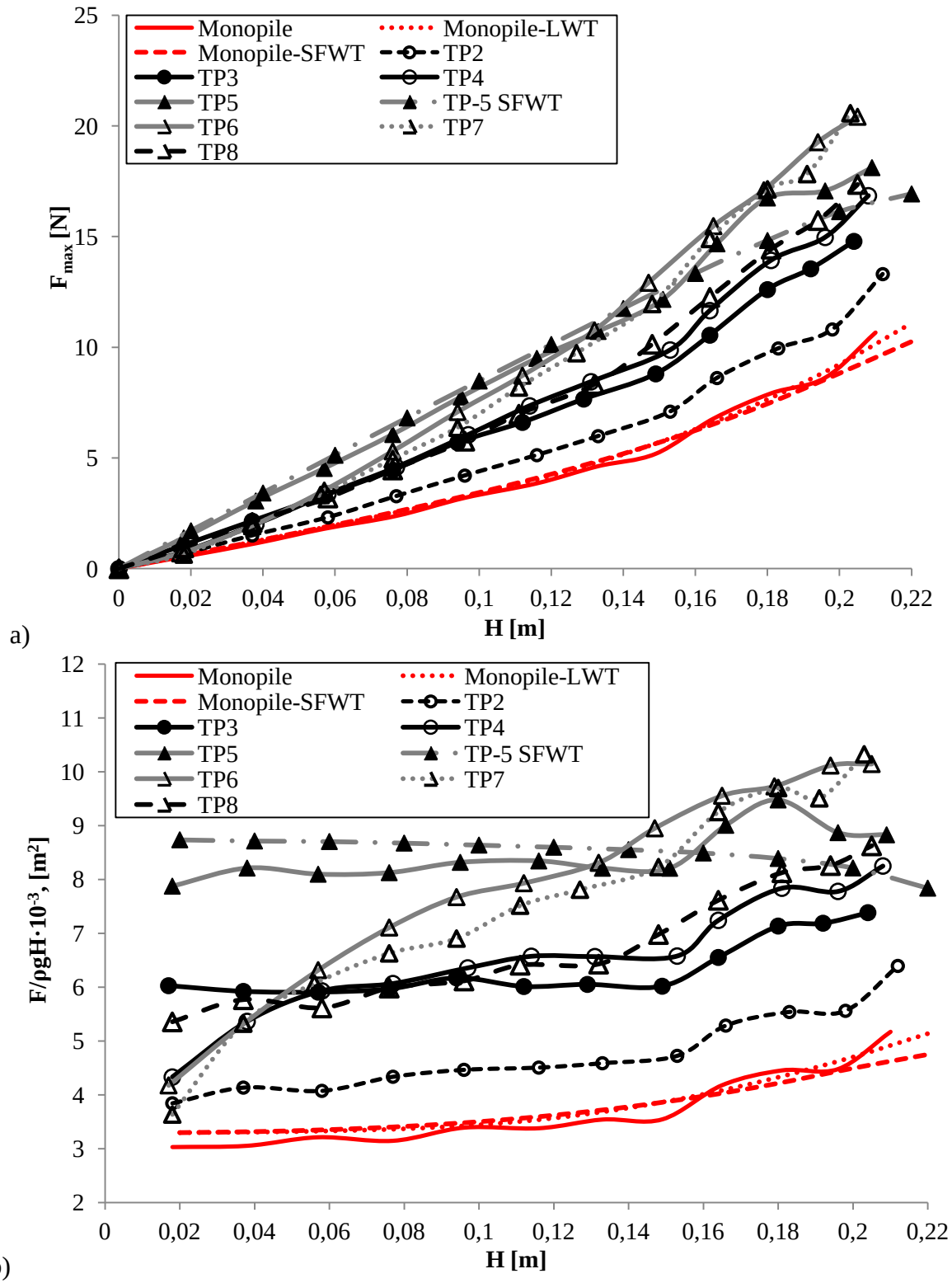

Figure 5. a) Average maximum peak forces vs. wave height (LWT: Linear wave theory; SFWT: Stream function wave theory), Morison load model. b) Average maximum peak forces vs. wave height normalized with ρgH.

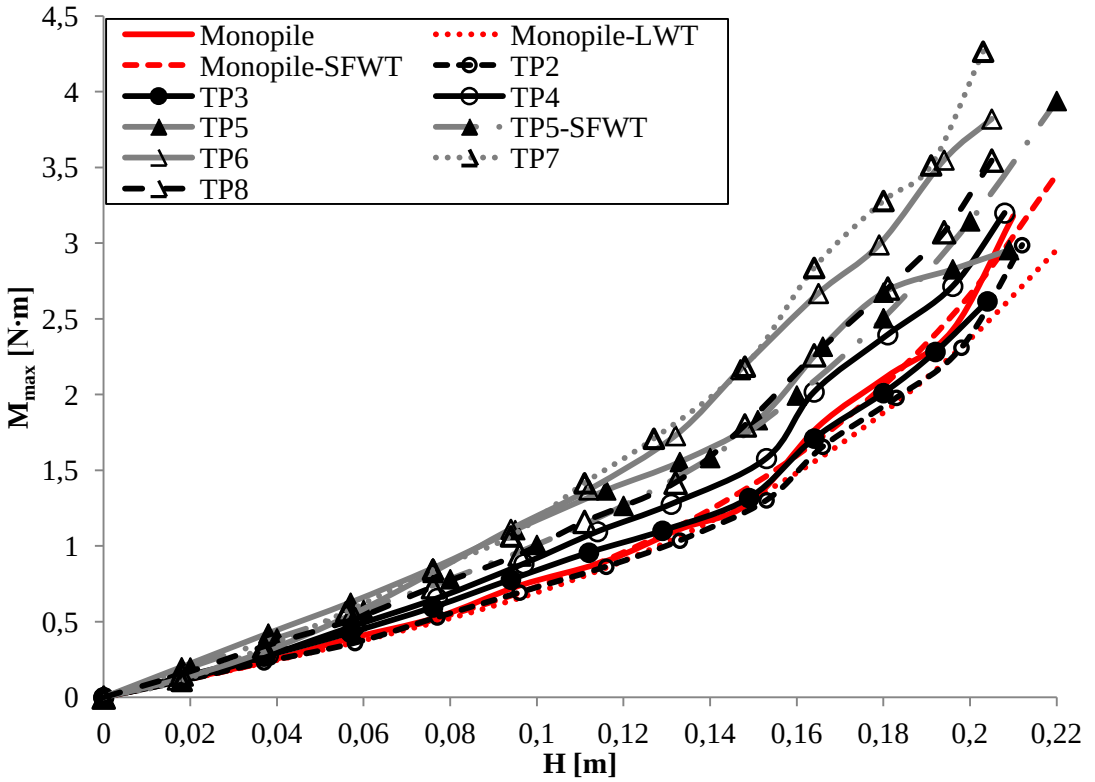

a)

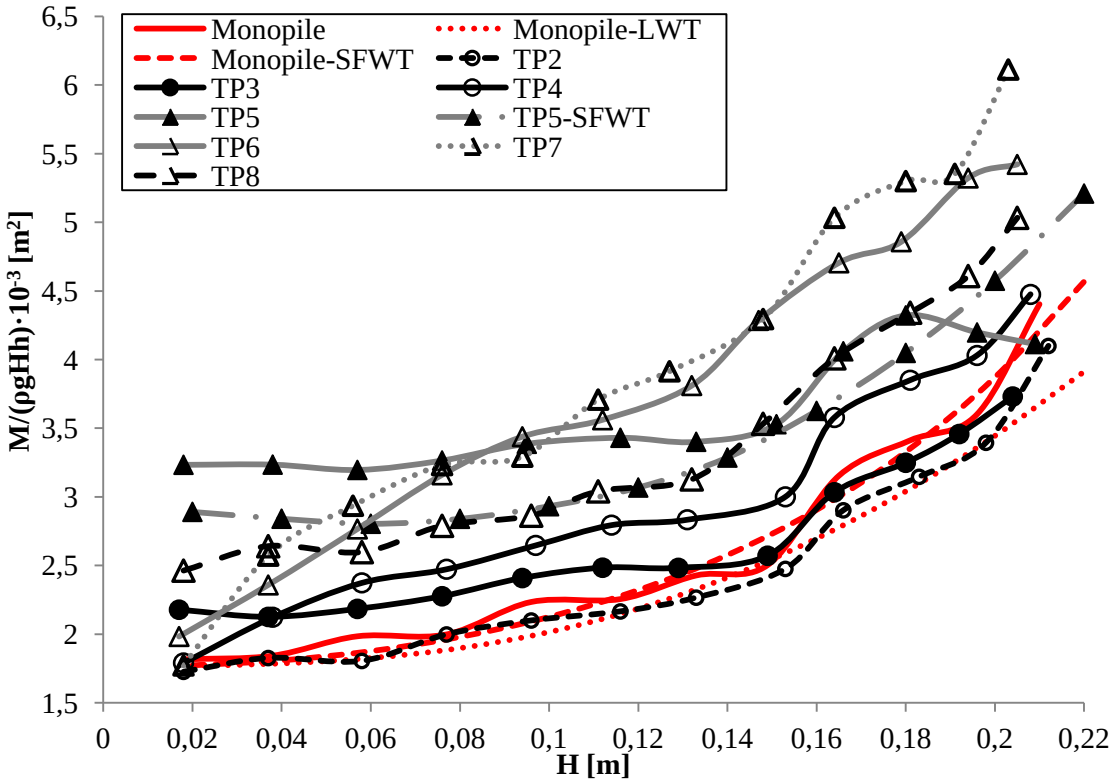

b)

Figure 6. a) Average maximum peak moments vs. wave height (LWT: Linear wave theory; SFWT: Stream function wave theory), Morison load model. b) Average maximum peak moments vs. wave height normalized with ρgHh.

C_M was estimated reasonably accurate and fit well in the area with inertia dominance (i.e. the small wave heights). Overall, a better fit of the experimental results was observed with the SFWT and, therefore, this theory was further used in the analysis of the wave forces on various TPs.

Furthermore, calculation of hydrodynamic loads on the solid conical model TP5 was included using the Morison equation and SFWT by dividing the height of the substructure into several discs of height Δh = 0.1 m with a constant value of the diameter with the load coefficients C_D = 0.8; C_M = 2. A good fit was achieved for the wave heights H < 0.16 m for the maximum peak forces (as shown in Figure 5), even though the maximum forces obtained from the tests were for the smallest waves lesser than the calculated. Generally, the experimental maximum moments were larger than the calculated moments using SFWT (see Figure 6). This might be explained by the flow of the water particles around conically-shaped models. In the experiments, the water particles will try to move upwards, as it is easier for the flow to pass the foundation, where the diameter is smaller (i.e. where D = 0.075 m). In the Morison equation it is, however, assumed that the water particles follow a path, in which each individual particle moves around the foundation at the same level. This is expected to be the reason for this observation. On the other contrary, the moments acting on TP2 were smaller than the moments acting on the monopile even though the forces acting on it were higher as earlier discussed in Section 3.2.

Comparison of the wave forces acting on the TPs shows that the best performance in terms of wave loads was achieved for the traditional design TP2 and solid doubly curved model TP3. The moments from the hydrodynamic loading acting on the models TP2 and TP3 were comparable to the moments from wave forces acting on the monopile (Figure 6). Cutaways introduced to the doubly curved model TP4 were efficient only for the small wave heights less than H = 0.06 m. Moreover, implementation of cutaways into the conical models TP6 and TP7 contributed to the reduction of wave forces, yet only at the wave heights smaller than $H \approx 0.13{-}0.15$ m, correspondingly (Figure 5). The explanation of this phenomenon is the following: for lower wave heights, inertia dominates. In contrast, for higher wave heights and, hence, larger wave crest velocity and KC numbers, the drag becomes important and the sharp cutaways create separation, contributing negatively to the wave force reduction.

Moreover, the reduction of the moments acting on the TP6 and TP7 was achieved only for the wave heights less than $H \approx 0.09{-}0.10$ m, respectively, (Figure 6) compared to the solid model TP5. In contrast, conical model TP8 with six streamlined circular elements was not as effective in terms of wave force reduction as the models TP6 and TP7 for the wave heights lower than H = 0.04 m, but it soon showed a better performance for the higher waves. Furthermore, model TP8 was efficient with respect to moment reduction for the wave heights up to H = 0.18 m, whereas the solid conical model TP5 showed a better performance for the higher waves.

In addition, maximum peak moments and forces were normalized with respect to the results for the reference case – monopile with D = 0.075 m − using the stream function wave theory (SFWT) selected as the one earlier providing the better fit. The experimental results for H = 0.24 m

were excluded from this study as the SFWT could not converge for this wave height and were plotted against wave heights as shown in Figures 7 to 8. The volume of the monopile and other TPs was calculated for the comparison of the normalized forces and moments for 35 cm water depth. The volume of the monopile was 1547 cm^3, doubly curved model TP3 − 1701 cm^3 (1.1 times the volume of the monopile), and truncated conical model TP5 − 4410 cm^3 (2.85 times the volume of the monopile).

Generally, the traditional transition piece TP2 showed the best performance in terms of wave force reduction (Figure 7) with 1.17−1.39 times the calculated value for the monopile using SFWT. The maximum normalized wave forces, acting on the doubly curved models TP3 and TP4 were 1.73 and 1.31 times the maximum force acting on the monopile calculated using SFWT for the wave height $H \approx 0.018$ m. Moreover, for the wave height $H \approx 0.21$ m they were 1.55 and 1.76 times the maximum force acting on the monopile.

The normalized force curve for the solid truncated conical model TP5 started much higher than for the models with cutaways TP6 and TP7 (see Figure 7) and was 2.39 times the maximum force acting on the monopile calculated using SFWT for TP5 vs. 1.20 and 1.10 times for TP6 and TP7, respectively. It is interesting to observe that for models TP6 and TP7 the force curves start very close to the force curve for TP2 and finish almost at the same point for TP6 and TP7, while the curve for TP6 lies higher than one for TP7, showing a positive effect of the smaller multiple cutaways. Initially, for the wave heights up to $H \approx 0.12$ m the normalized force curve for TP5 reached a plateau of almost constant value of 2.32−2.48 times the reference case. For the truncated conical models TP6−TP7, a positive effect of the cutaways was more pronounced for the small wave heights.

Moreover, steep growth was detected for these models for both the normalized force and moment curves for the wave heights up to $H \approx 0.16$ m and $H \approx 0.08$−0.1 m, respectively, followed by a steady decay before almost merging at $H \approx 0.22$ m for the normalized force curves. For the model TP5 decay of the normalized force curve resulted in a better performance in terms of reduction of hydrodynamic loading for the waves higher than $H \approx 0.15$ m compared to the models TP6−TP7. The maximum normalized wave forces, acting on TP5, TP6 and TP7 were 1.90, 2.14 and 2.15 times those for the wave height $H \approx 0.2$−0.21 m. Furthermore, a steady decay of the normalized moment curve was observed for TP5 and a better performance was achieved compared to the models TP6−TP7 when the wave heights were larger than $H \approx 0.12$ m. Model TP8 with streamlined elements performed better than the models TP5−TP7 and was 1.62−1.92 times the maximum force acting on the monopile.

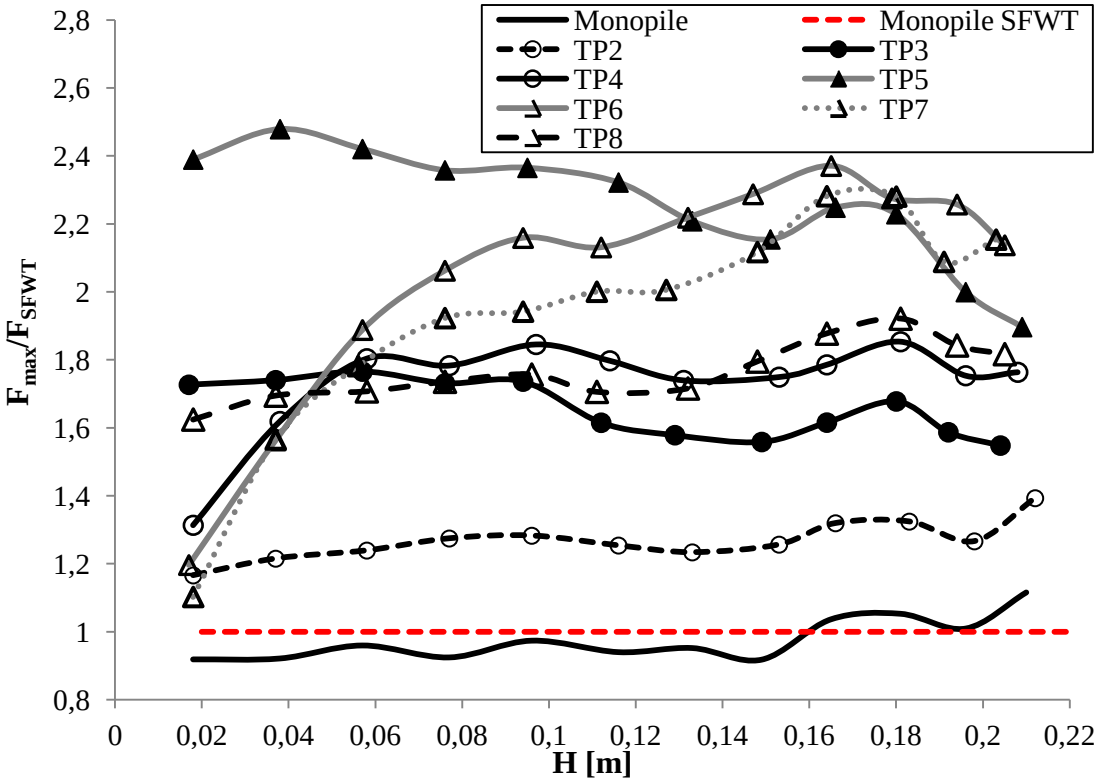

Figure 7. Maximum peak forces vs. wave height normalized with results for monopile and stream function wave theory (SFWT)

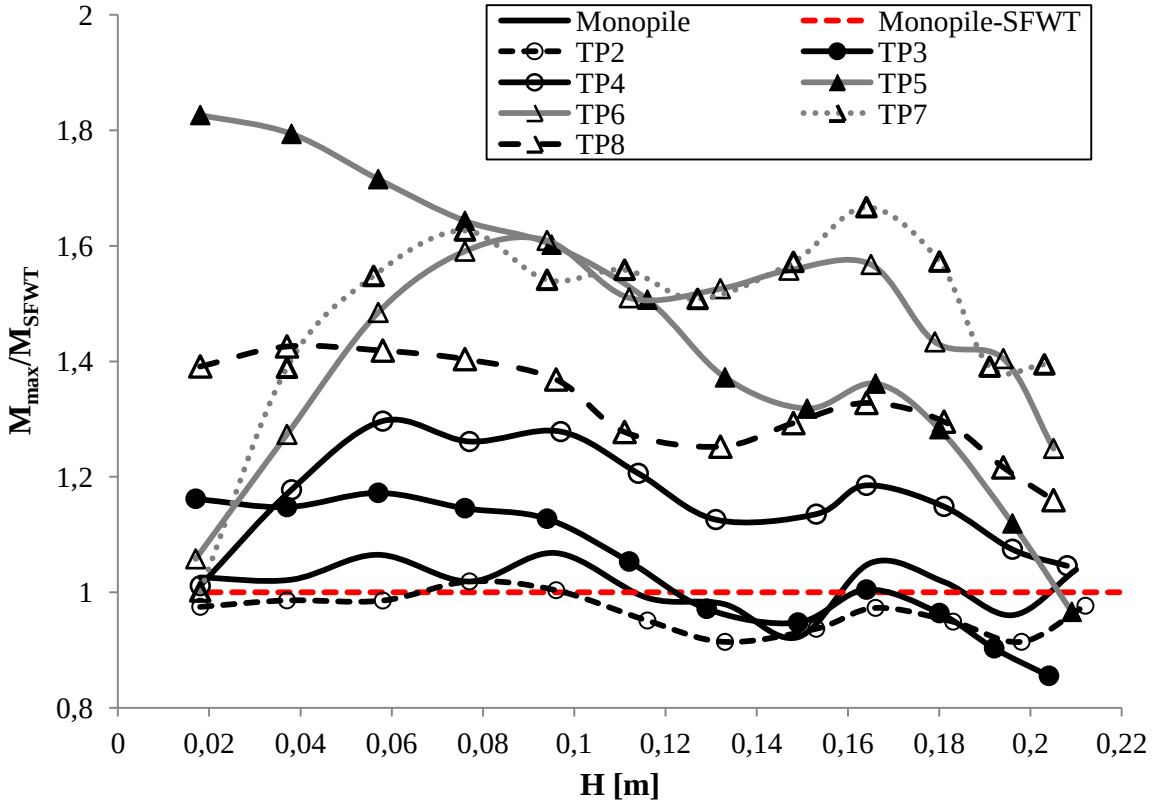

Figure 8. Maximum peak moments vs. wave height normalized with results for monopile and stream function wave theory (SFWT)

6.2. Irregular waves

Maximum forces and moments for the TP models are presented in Table 3. In Figure 1 of the appendix the points of attack and the moments are presented for all the models as functions of the horizontal forces for two assigned irregular wave loading scenarios: H_s = 0.095 and H_s = 0.115 m, T_p =1.4 s in model scale corresponding to H_s = 9.5 and H_s = 11.5 m, T_p = 14 s in prototype conditions. Figure 1 of the appendix shows that the maximum horizontal wave forces did not attack at the highest points of application. Moreover, the maximum moment normally occurred at the same time as the maximum horizontal force. Therefore, transition pieces must be dimensioned for the maximum horizontal force corresponding to the point of application, since this also gives the maximum moment. On the contrary, in the design of the substructures where the maximum horizontal force does not attack at the highest point of application, combinations of the horizontal forces and moments must be used, as it might be not clear which combination is worst. Moreover, the resultant horizontal forces have attack points that lie below the mean water level due to inertia dominance and also due to the largest volume of the lower part of most foundations. Another expected observation is that the positive horizontal forces were generally larger than the negative and attacked slightly higher. A final observation from Figure 1 in the appendix is that there were some points where the horizontal forces were substantially greater than the remaining points and formed additional curves parallel to the main solid-bodied curve. This could have been due to extreme waves the occurred during the experiments.

Table 3. Maximum forces and moments for the TP models.

Model	Irregular wave conditions				Max. Force F [N]	$F_{2\%\ Max.Peaks}$ [N]	Max. Mom. M [N·m]	$M_{2\%\ Max.Peaks}$ [N·m]
	H_s [m]	T_s [s]	$H_{2\%}$ [m]	H_{max} [m]				
Monopile	0.091	1.331	0.129	0.170	7.64	5.009	1.957	1.227
	0.108	1.337	0.148	0.194	9.714	6.024	2.752	1.515
TP2	0.091	1.31	0.128	0.199	11.99	6.119	2.578	1.15
	0.107	1.324	0.141	0.197	10.71	7.489	2.269	1.39
TP3	0.093	1.33	0.126	0.161	10.34	8.373	1.584	1.23
	0.101	1.326	0.136	0.192	13.08	9.49	2.078	1.43
TP4	0.091	1.332	0.119	0.170	11.08	8.582	1.839	1.348
	0.104	1.325	0.138	0.170	12.75	9.919	2.1	1.608
TP5	0.089	1.331	0.121	0.184	18.51	11.21	3.013	1.679
	0.104	1.352	0.137	0.187	18.51	12.83	3.027	1.963
TP6	0.093	1.329	0.123	0.160	14.84	10.26	2.542	1.744
	0.108	1.325	0.147	0.177	17.75	12.65	3.338	2.206
TP7	0.086	1.341	0.119	0.150	14.64	9.814	2.856	1.758
	0.099	1.311	0.135	0.172	16.87	11.47	3.211	2.163
TP8	0.094	1.337	0.127	0.166	12.37	8.76	2.437	1.542
	0.107	1.338	0.146	0.175	14.45	10.13	2.977	1.89

According to Table 3, the highest maximum wave force of F_{Hmax} = 18.51 N was acting on the truncated conical solid TP5 for both loading cases, while the lowest maximum wave forces of F_{Hmax}= 7.64 and 9.714 N were applied to the a reference case for H_s = 0.091 and 0.108 m, respectively. Moreover, the maximum horizontal forces, acting on the traditionally designed TP2 and doubly curved models TP3 and TP4, were 1.57, 1.35 and 1.45 times the maximum force acting on the monopile for H_s = 0.091−0.093 m, and 1.10, 1.35 and 1.31 times higher, correspondingly, for H_s = 0.101−0.107 m. The cutaways, actually, lead to a wave force increase in model TP4 for H_s = 0.091 m and decreased the hydrodynamic loading for H_s = 0.104 m.

The maximum wave forces, acting on the truncated conical models TP5, TP6 and TP7, were 2.42, 1.94 and 1.92 times the maximum force acting on the monopile for H_s = 0.086−0.093 m, and 1.91, 1.83 and 1.74 times higher, correspondingly, for H_s = 0.099−0.108 m. Model TP8 with streamlined elements showed better performance in terms of wave load reduction on the truncated conical shaped substructures with 1.62 and 1.49 times the maximum force acting on the monopile for H_s = 0.094 and 0.107 m, respectively. Generally, the traditional design TP2 showed the best performance with respect to hydrodynamic loading reduction for significant wave height H_s = 0.107 m. Moreover, the second best result was achieved for the doubly curved models TP3 and TP4, with the porous model TP4 being more efficient for the lower significant wave height H_s = 0.091 m, and the solid model TP3 showing the better results for both significant wave heights.

As for the ratios of the maximum moments acting on the TP models to the maximum moments acting in the reference case (monopile), the following results were achieved: 1.32, 0.81, 0.94, 1.54, 1.30, 1.46, and 1.25, for TP2, TP3, TP4, TP5, TP6, TP7, and TP8, respectively, for H_s = 0.086−0.094 m; and 0.82, 0.76, 0.76, 1.10, 1.21, 1.17, and 1.08, respectively, for H_s = 0.099−0.108 m. Based on these results, overall, the doubly curved models TP3 and TP4 showed the best performance, while the solid model TP3 showed a slightly better result for a lower significant wave height. Comparing conical models TP5-TP8, the best performance was observed for TP8 with streamlined elements. Furthermore, the cutaways were efficient in terms of reduction of moments from the wave forces on TP6 and TP7 for the lower significant height and increased the moments compared to the solid model TP5 for the higher significant wave height.

Results of the wave experiments are compared and shown in Table 4 based on the maximum forces and moments from regular and irregular wave loading. The results for the maximum forces and moments were moderately close for all cases, except for the models TP5 and TP7, where a small deviation was observed.

Table 4. Comparison of the results of maximum forces and moments from irregular and regular waves

Model	Irregular wave conditions			Regular wave conditions		
	H_{max} [m]	Max. force F [N]	Max. mom. M [N•m]	H_{max} [m]	Max. force F_{max} [N]	Max. mom. M_{max} [N•m]
Monopile	0.170	7.64	1.957	0.165	6.77	1.789
	0.194	9.714	2.752	0.196	8.618	2.427
TP2	0.199	11.99	2.578	0.198	10.81	2.31
	0.197	10.71	2.269	0.198	10.81	2.31
TP3	0.161	10.34	1.584	0.164	10.55	1.71
	0.192	13.08	2.078	0.192	13.55	2.282
TP4	0.170	11.08	1.839	0.164	11.66	2.017
	0.170	12.75	2.1	0.164	11.66	2.017
TP5	0.184	18.51	3.013	0.18	16.75	2.674
	0.187	18.51	3.027	0.196	17.07	2.828
TP6	0.160	14.84	2.542	0.165	15.48	2.668
	0.177	17.75	3.338	0.179	17.1	2.989
TP7	0.150	14.64	2.856	0.148	11.96	2.185
	0.172	16.87	3.211	0.18	17.14	3.279
TP8	0.166	12.37	2.437	0.164	12.26	2.26
	0.175	14.45	2.977	0.181	14.44	2.701

6.3. Modelling inaccuracy

This paper presented the hydrodynamic experiments performed in the wave flume. Several errors can be induced by conducting the wave experiments in a small-scale laboratory facility (see, e.g. Høgedal [19]). The limited width (B) of the wave flume can cause an undesirable blockage effect which though is negligible when $\frac{B}{D}$ >5−10.

Another observation should be made regarding fitting the forces and the moments for the reference case (monopile) based on the Morison equation and linear wave theory or stream function wave theory. In this research, the current velocity U in the flume was assumed to be zero. On the other hand, since the wave flume represents a closed basin, the discharge q has to be zero when the return flow is fully established in the flume (U < 0). It will eventually happen, however, only after some waves. Therefore, there might have been a little difference on the results if q = 0 was used instead.

Finally, the measurements of the wave forces acting on the models TP2, TP4 and TP6−TP8 are anticipated to be dependent on the orientation of the cutaways towards the current in the wave flume, but this effect was not studied.

7. Conclusions

The aim of the present work was to compare hydrodynamic loading on the various shapes of the transition pieces in deep water wave environment, to suggest the shape that could minimize the wave forces acting on the substructures and to study the effect of implementation of cutaways on the wave loading.

The experimental results for the monopile matched well with the theoretical values for the forces and moments calculated using the Morison equation and stream function wave theory (SFWT). A traditional solution for the transition piece and a solid doubly curved model showed the smallest increase in loads compared to the monopile.

Cutaways in the transition piece were quite effective for the low wave heights, but with an increase of the wave height, i.e. when the drag term in the Morison equation becomes important, they were not further effective with respect to wave force reduction. In general, cutaways have shown to have the negative effect on the forces compared to the solid substructures of the same shape. However, cutaways introduced in the form of streamlined columns, or legs, have shown to reduce the forces on the conical shape and, thus, should be studied further. It can be also concluded that the form of the cutaways for the transition pieces should be optimized not only with respect to structural performance, cost or material savings, but also with respect to reduction of the hydrodynamic loading on these substructures.

REFERENCES

[1] Nezhentseva, A., Andersen, L.V., Ibsen, L.B. and Sørensen, E.V. (2010). *Material composition of bucket foundation transition pieces for offshore wind turbines.* CST2010: The Tenth International Conference on Computational Structures Technology: Valencia, Spain, Paper 109.

[2] Nezhentseva, A., Andersen, L.V., Ibsen, L.B. and Sørensen, E.V. (2011). *Performance-based design optimization of a transition piece for bucket foundations for offshore wind turbines:* The Thirteenth International Conference on Civil, Structural and Environmental Engineering Computating: Chania, Crete, Greece, Paper 96.

[3] Mayer, S., Garapon, A. and Sørensen, L.S. (1998). *A fractional step method for unsteady free-surface flow with application to non-linear wave dynamics*. Intl. Journal for Numerical Methods in Fluids, Vol. 28, No. 2, pp. 293-315.

[4] Emarat, N., Christensen, E. D., Forehand, D. I. M. and Mayer, S. (2000). *A study of plunging breaker mechanics by PIV measurements and a Navier-Stokes solver*. In Proceedings of the 27th Int. Conf. on Coastal Eng., ASCE, Sydney, Australia, Vol. 1, pp. 891-901.

[5] Nielsen, KB, and Mayer, S. (2004). *Numerical prediction of green water incidents*. Ocean Engineering, Vol 31, pp. 363-399.

[6] Christensen E.D. (2006) *Large eddy simulation of spilling and plunging breakers*, Coastal Engineering, Volume 53, Issues 5-6, pp. 463-485.

[7] Bredmose H., Skourup J., Hansen E.A., Christensen E.D., Pedersen L.M. and Mitzlaft A. (2006) *Numerical reproduction of extreme wave loads on a gravity wind turbine foundation*. Proceedings of OMAE 25th International Conference on Offshore Mechanics and Arctic Eng., 4-9 June 2006, Hamburg, Germany.

[8] Christensen E.D., Bredmose H. and Hansen E.A. (2005) *Extreme wave forces and wave run-up on offshore wind-turbine foundations.* Copenhagen Offhore Wind 2005, pp. 1-10.

[9] Li Y.-C., Wang F.-L. and Wang H.-R. (1993) *Wave-Current Forces On Vertical Piles In Side-by-Side Arrangement.* International Journal of Offshore and Polar Engineering. Vol. 3, No.3, 6p.

[10] Markus D., Hojjat M. Wüchner R. and Bletzinger K.-U. (2012) *A Numerical Wave Channel for the Design of Offshore Structures with Consideration of Wave-Current Interaction.* Technische Universität München, Munich, Germany. Proceedings of the Twenty-second International Offshore and Polar Engineering Conference Rhodes (ISOPE-2012), Greece, June 17–22, pp. 695-702.

[11] Sarpkaya T. *Quasi-2-D Forces on a Vertical Cylinder in Waves.* Journal of Waterway, Port, Coastal and Ocean Engineering, Vol. 110, No. 1, February 1984, pp. 120-123. Discussion to paper by Stansby P.K., Bullock G.N. and Short I., February, 1983, WW, Vol. 109, No.1.

[12] Sarpkaya T. and Isaacson M. (1981) *Mechanics of Wave Forces on Offshore Structures.* Van Nostrand Reinholdt Company Inc.

[13] Chakrabarti S.K. (1987) *Hydrodynamics of Offshore Structures*. Computational Mechanics Publications, Southampton, England.

[14] Chakrabarti S.K. (1990) *Nonlinear Methods on Offshore Engineering*. Elsevier

[15] Peeringa J.M. (2004) *Wave Loads on Offshore Wind Turbines; Feasibility study using results of wave experiments executed by Electricité de France (EDF),* ECN-C-04-042.

[16] Larsen B.J and Frigaard P. (2005) *Wave Forces on Windturbine Foundations: for the London Array*. Department of Civil Engineering, Aalborg University, Denmark. Hydraulics and Coastal Engineering; Vol. 30, 37p.

[17] Mo W., Irschik K., Oumeraci H. and Liu P. L.-F. (2007) *A 3D Numerical Model for Computing Non-Breaking Wave Forces on Slender Piles*. Journal of Engineering Mathematics, Vol. 58, pp.19-30

[18] Zhang W. (2009) *An Experimental Study and a Three-Dimensional Numerical Wave Basin Model of Solitary Wave Impact on A Vertical Cylinder*. A thesis submitted to Oregon State University in partial fulfilment of the requirements for the degree of Master of Ocean Engineering, 344 p.

[19] Høgedal M. (1993) *Experimental Study of Wave Forces on Vertical Circular Cylinders in Long and Short Crested Sea.* PhD thesis. Hydraulics & Coastal Engineering Laboratory, Department of Civil Engineering, Aalborg University, 232 p.
[20] Wienke, J., Sparboom, U. and Oumeraci, H. (2004) *Theoretical formulae for wave slamming loads on slender circular cylinders and application for support structures of wind turbines.* Proceedings 29th International Conference on Coastal Engineering (ICCE), ASCE, Volume 4, Lisbon, Portugal, pp. 4018-4026.
[21] De Vos L. , Frigaard P. and De Rouck J. (2007) *Wave Run-Up on Cylindrical and Cone Shaped Foundations for Offshore Wind Turbines.* Coastal Engineering, Vol. 54, Nr. 1, pp. 17-29.
[22] Lykke Andersen T. , Frigaard P., Damsgaard, M. L. and De Vos, L. *Wave Run-up on Slender Piles in Design Conditions: model tests and design rules for offshore wind.* Coastal Engineering, Vol. 58, Nr. 4, 2011, pp. 281-289.
[23] Lykke Andersen T. , Frigaard P. (2006) *Horns Rev II, 2-D Model Tests : wave run-up on pile* . Department of Civil Engineering, Aalborg University, Aalborg, Denmark, 43pp.
[24] Modridge G.R. and Jamieson W.W. (1976) *Wave Forces on Square Caissons.* In Proceeding of the 135th Coastal Engineering Conference AMSE, Ch. 133, pp. 2271-2289.
[25] MacCamy R.C. and Fuchs R.A. (1954) *Wave Forces on Piles: A Diffraction Theory.* U.S. Army Corps of Engineering, Beach Erosion Board, Technical Memorandum No. 69
[26] Au M.C. and Brebbia C.A. (1983) *Diffraction of Water Waves for Vertical Cylinders Using Boundary Elements.* Appl. Math. Modelling Vol. 7, pp.106-114.
[27] Zhu S. and Moule G. (1994) *Numerical Calculation of Forces Induced by Short-Crested Waves on a Vertical Cylinder of Arbitrary Cross-Section.* Ocean Engineering, Vo. 21, No.7 pp.645-662.
[28] Nezhentseva A., Lykke Andersen T., Andersen L.V. and Ibsen L.B. *Scour Development at Bucket Foundations for Offshore Wind Turbines*, Aalborg University. Department of Civil Engineering, Aalborg, Denmark, 2012. 23p. (DCE Technical Memorandum; No. 29).
[29] Hansen E.A. and Christensen E.D. (2007) *Scour Holes or Scour Protection around Offshore Wind Turbine Foundations: Effect on Loads*. Part of: Conference proceedings of EWEC 2007, Presented at: 2007 European Wind Energy Conference and Exhibition, Milan
[30] Frigaard P., Hansen E.A., Christensen E.D. and Jensen M.S. (2005) *Effect of Breaking Waves on Scour Processes around Circular Offshore Wind Turbine Foundations*. NWTC External Web Site. National Wind Technology Center.
[31] DNV-OS-J101 (2007) *Det Norske Veritas: Design of Offshore Wind Turbine Structures,* Offshore Standard, 142pp.
[32] Airy, G. B. (1845) *Tides and Waves, Encyc. Metrop.* Article 102.
[33] Stokes G.G. (1847) *On the Theory of Oscillatory Waves.* Transactions of the Cambridge Philosophical Society 8, pp. 441-455.
[34] Dean R.G. (1965) *Stream function representation of nonlinear ocean waves*. Journal of Geophysical Research, Vol. 70, No.18: pp. 4561–4572.
[35] LeMehaute B, Divoky D, and Lin A. (1968) *Shallow Water Waves: A Comparison of Theories and Experiments*. Proceedings, 11th Conference on Coastal Engineering, American Society of Civil Engineers, London, pp. 86-107.
[36] Dean R.G. (1974) *Evaluation and Development of Water Wave Theories for Engineering Application*. Special Report No. 1, U.S. Army Coastal Engineering Research Center, Ft. Belvoir, VA (2 Vols).
[37] Fenton J.D. (1979) *A high-order cnoidal wave theory* J. Fluid Mech., Vol. 94, Part1, pp. 129-161.
[38] Morison J.R.,O'Brian M.P., Johnson J.W. and Schaaf S.A. (1950) *The Force Exerted by Surface Waves on Piles.* Petroleum Transactions (American Institute of Mining Engineers), Vol. 189, pp.149-154.
[39] Madsen P.A., Bingham H.B. and Liu H. (2002) *A New Boussinesq Method for Fully Nonlinear Waves From Shallow to Deep Water.* Journal of Fluid Mechanics, vol. 462, pp.1-30.

[40] Wienke J. (2001) *Druckschlagbelastung auf schlanke zylindrische Bauwerke durch brechende Wellen: theoretische und großmaßstäbliche Laboruntersuchungen* PhD thesis, Technischen Universität Carolo-Wilhelmina, Braunschweig, Germany. http://rzbl04.biblio.etc.tu-bs.de:8080/docportal/content/below/index.xml

[41] DNV-RP-C205 (2010) *Det Norske Veritas: Environmental Conditions and Environmental Loads,* Recommended Practice, 124pp.

[42] DRAFT by Grontmij/Carl Bro (2009) *Carbon Trust OWA Offshore Wind Farm Foundations UK Round 3. Design Basis. Version 2.*

[43] Schäffer H.A. (1996) *Second order wavemaker theory for irregular waves*. Ocean Engineering 23 (1), pp. 47-88.

[44] ISO 19901-1:2005-11 (E) *Petroleum and natural gas industries - Specific requirements for offshore structures -Part 1: Metocean design and operating considerations.*

[45] Isaacson M. and Baldwin J. (1990) *Random Wave Forces Near Free Surface*. J. Waterway, Port, Coastal, Ocean Eng., 116(2), pp. 232–251.

[46] Unal M. F. and Rockwell D. (1988) *On vortex formation from a cylinder. Part 1. The initial instability.* Journal of Fluid Mechanics, Vol. 190, pp. 491–512.

[47] Lin J.-C., Towfighi J. and Rockwell D. (1995) *Instantaneous structure of near-wake of a cylinder: on the effect of Reynolds number.* Journal of Fluids and Structures, Vol. 9, pp. 409–418.

[48] Blevins R.D. (1977) *Flow-induced vibration.* Van Nostrand Reinhold Company, New York.

[49] Swan C. (1990) *Wave kinematics within crest to trough region.* Environmental Forces on Offshore Structures and their Prediction, vol. 26. Society for Underwater Technology. Kluwer Academic Publishers, pp. 45-60.

[50] Burcharth H.F. (2002) *Strøm- og bølgekræfter på stive legemer*, Second edition, Aalborg University, Department of Civil Engineering, Aalborg, Denmark, 44pp.

[51] Henderson A. R. and Zaaijer M.B. (2002) *Hydrodynamic Loading of Compact Structures and the Effect on Foundation Design*. Marine Renewable Energy Conference (MAREC), Newcastle, UK.

[52] Lykke Andersen T. and Frigaard P. (2011) *Lecture Notes for the Course in Water Wave Mechanics.* Department of Civil Engineering, Aalborg University, Denmark, ISSN 1901-7286, (DCE Lecture Notes No.16), 116pp.

[53] Newman, J.N., Lee, C.H. and Korsmeyer, F.T. (1995) *WAMIT version 5.3. A Radiation-Diffraction Panel Program for Wave-body Interactions*. Dept. of Ocean Eng., MIT, Cambridge, MA.

[54] Laya E., Connor J., and Sunder S. (1984). *Hydrodynamic Forces on Flexible Offshore Structures.* Journal of Engineering Mechanics, Vol. 110, Issue 3, pp. 433–448.

APPENDIX

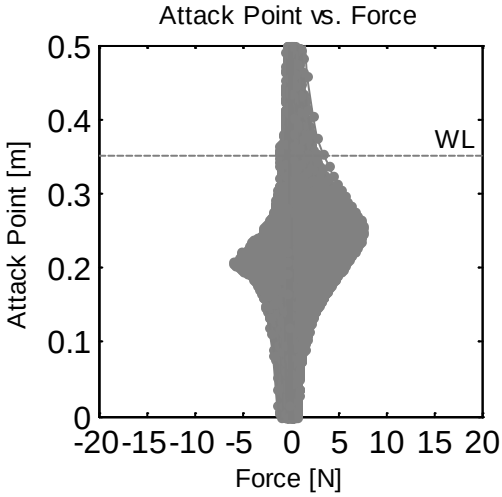

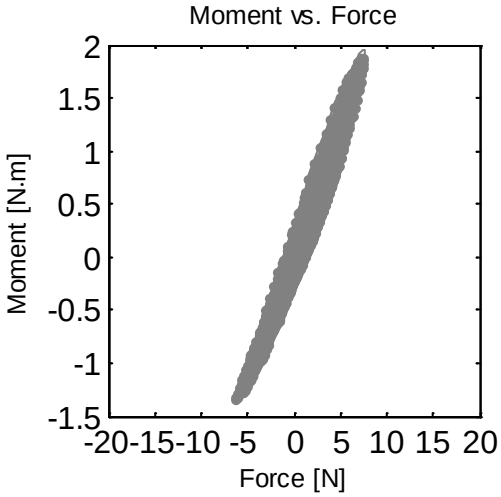

(1.1)

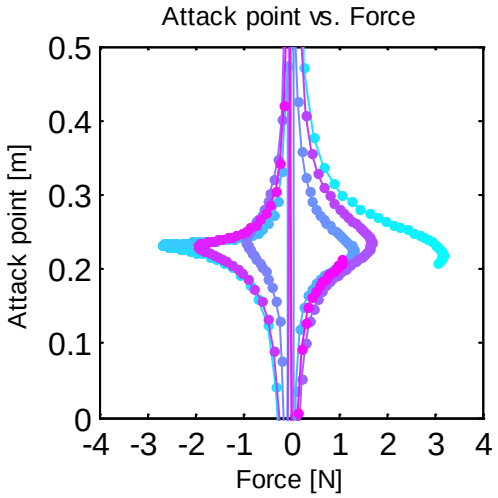

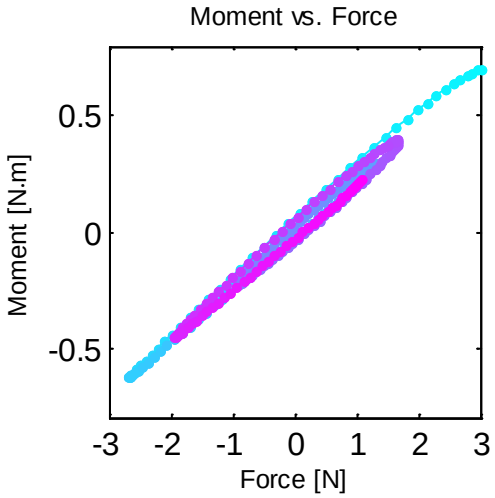

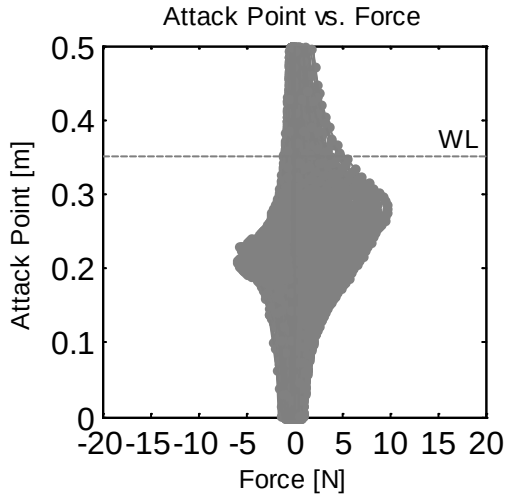

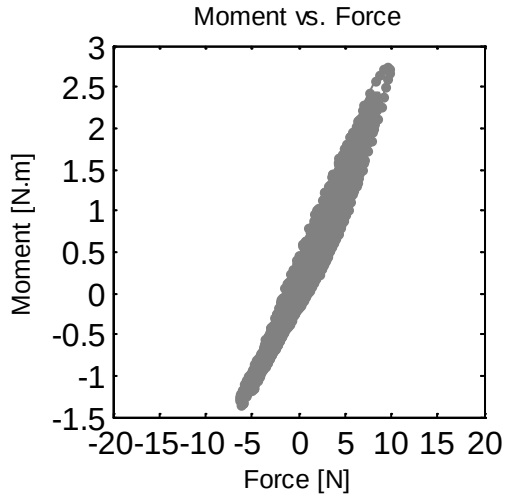

(1.2)

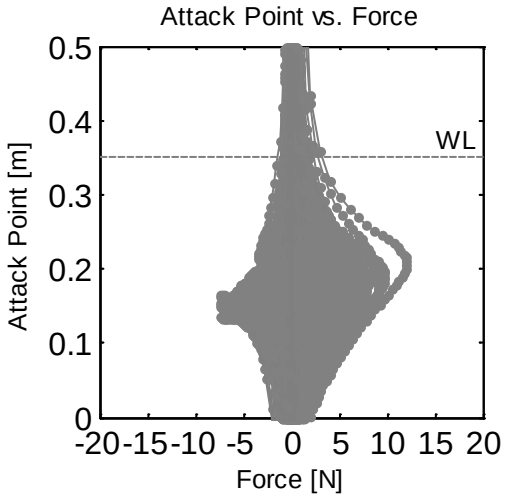
Attack Point vs. Force
Attack Point [m]
Force [N]
WL
0.5
0.4
0.3
0.2
0.1
0
-20 -15 -10 -5 0 5 10 15 20

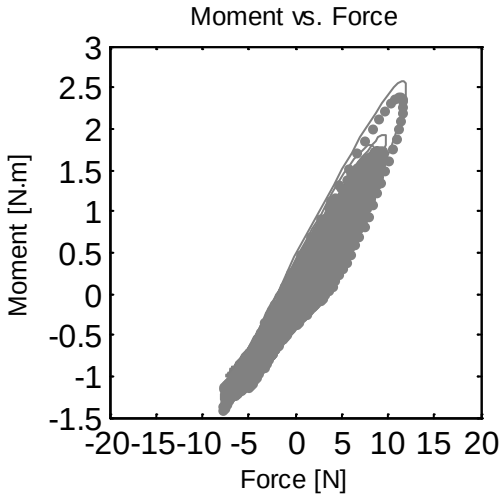
Moment vs. Force
Moment [N.m]
Force [N]
3
2.5
2
1.5
1
0.5
0
-0.5
-1
-1.5
-20 -15 -10 -5 0 5 10 15 20

(2.1)

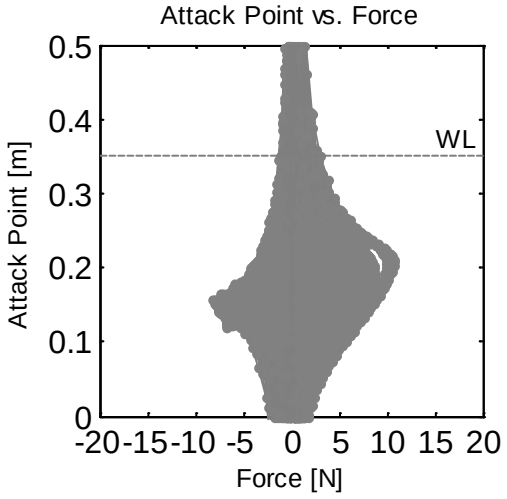
Attack Point vs. Force
Attack Point [m]
Force [N]
WL
0.5
0.4
0.3
0.2
0.1
0
-20 -15 -10 -5 0 5 10 15 20

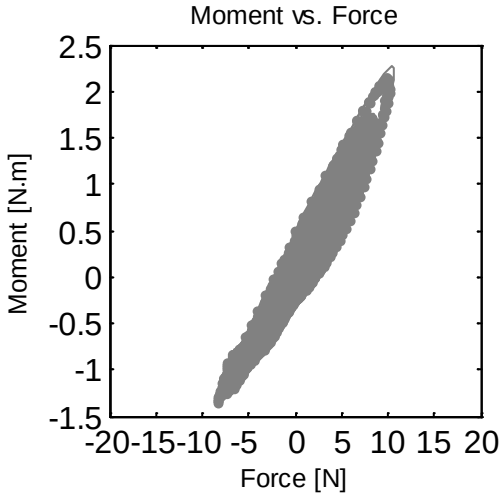
Moment vs. Force
Moment [N.m]
Force [N]
2.5
2
1.5
1
0.5
0
-0.5
-1
-1.5
-20 -15 -10 -5 0 5 10 15 20

(2.2)

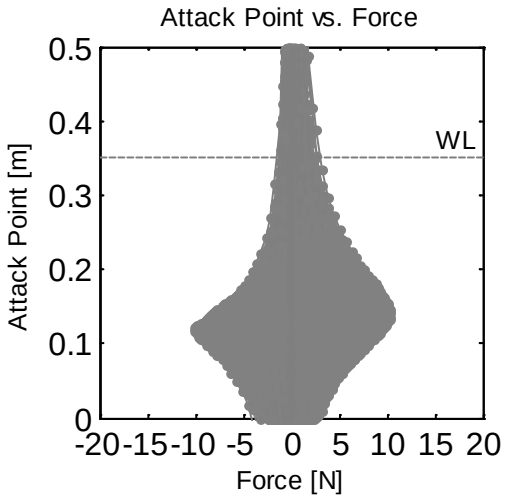
Attack Point vs. Force
Attack Point [m]
Force [N]
WL
0.5
0.4
0.3
0.2
0.1
0
-20 -15 -10 -5 0 5 10 15 20

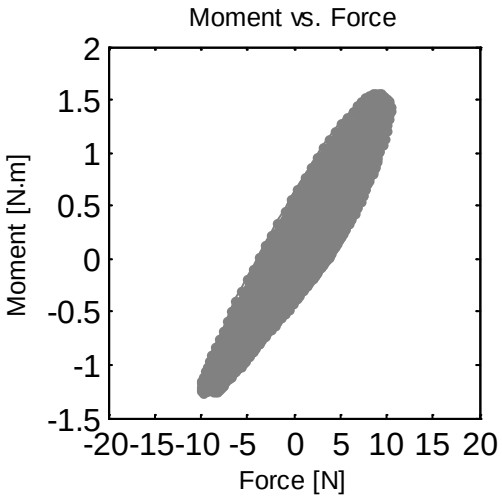
Moment vs. Force
Moment [N.m]
Force [N]
2
1.5
1
0.5
0
-0.5
-1
-1.5
-20 -15 -10 -5 0 5 10 15 20

(3.1)

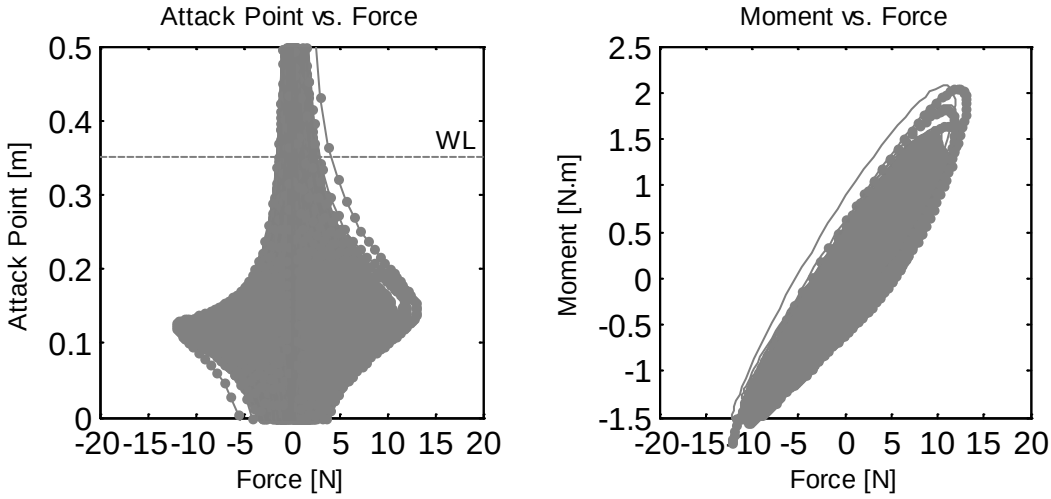
Attack Point vs. Force
Attack Point [m]
Force [N]
WL
Moment vs. Force
Moment [N.m]
Force [N]

(3.2)

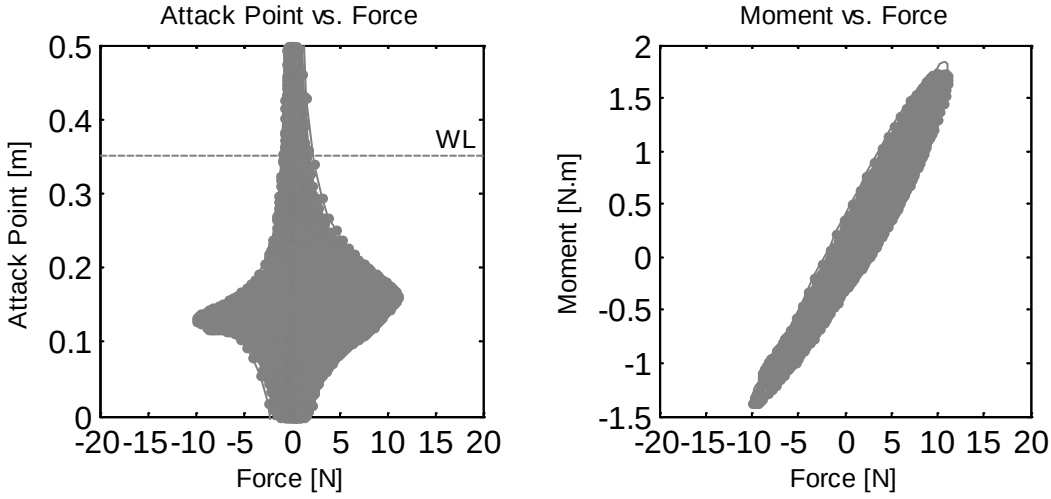
Attack Point vs. Force
Attack Point [m]
Force [N]
WL
Moment vs. Force
Moment [N.m]
Force [N]

(4.1)

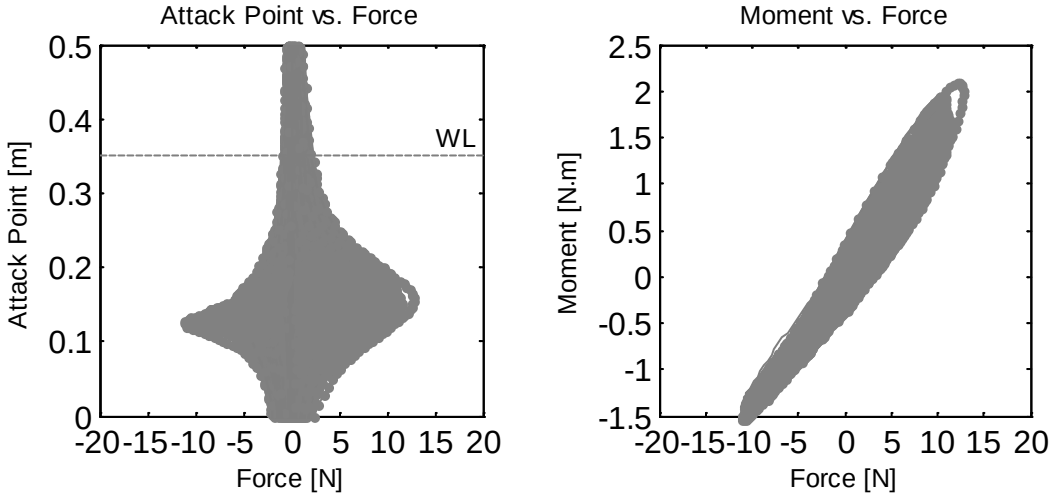
Attack Point vs. Force
Attack Point [m]
Force [N]
WL
Moment vs. Force
Moment [N.m]
Force [N]

(4.2)

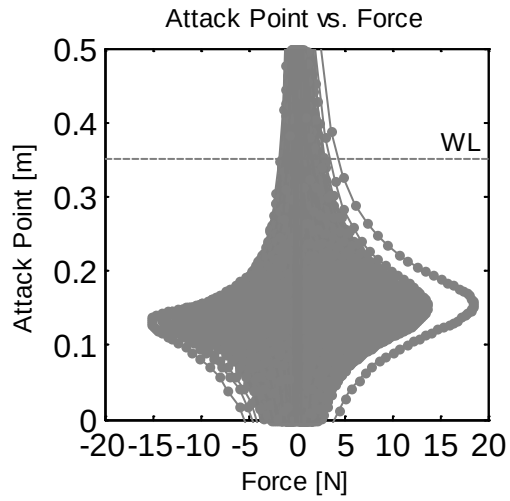
Attack Point vs. Force
Attack Point [m]
Force [N]
WL
0.5
0.4
0.3
0.2
0.1
0
-20 -15 -10 -5 0 5 10 15 20

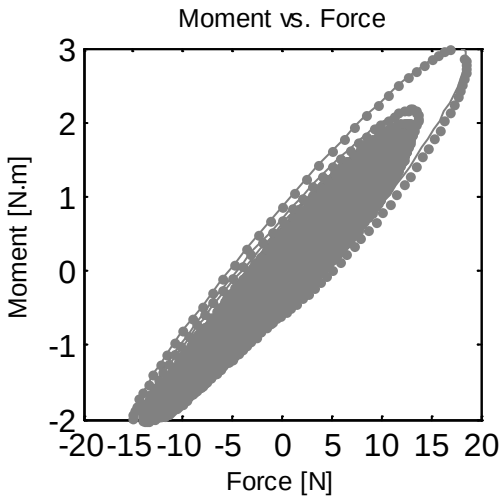
Moment vs. Force
Moment [N.m]
Force [N]
3
2
1
0
-1
-2
-20 -15 -10 -5 0 5 10 15 20

(5.1)

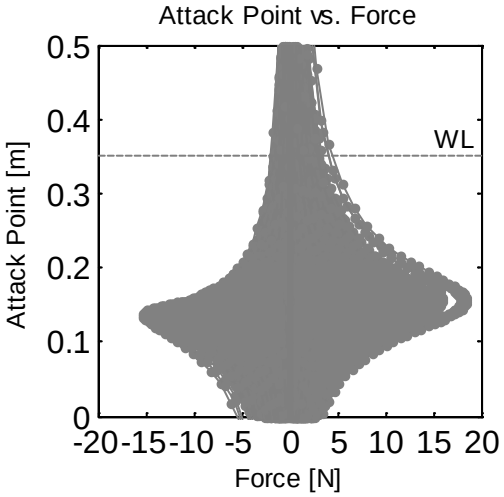
Attack Point vs. Force
Attack Point [m]
Force [N]
WL
0.5
0.4
0.3
0.2
0.1
0
-20 -15 -10 -5 0 5 10 15 20

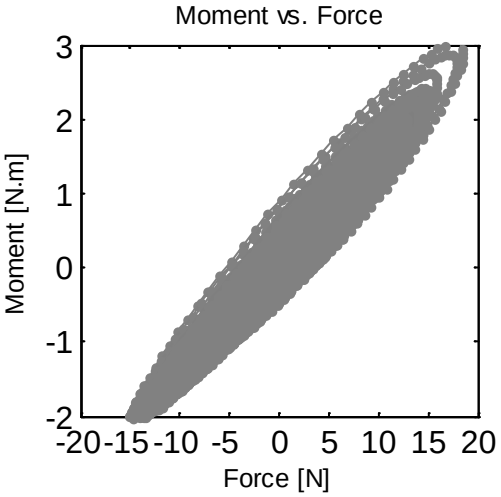
Moment vs. Force
Moment [N.m]
Force [N]
3
2
1
0
-1
-2
-20 -15 -10 -5 0 5 10 15 20

(5.2)

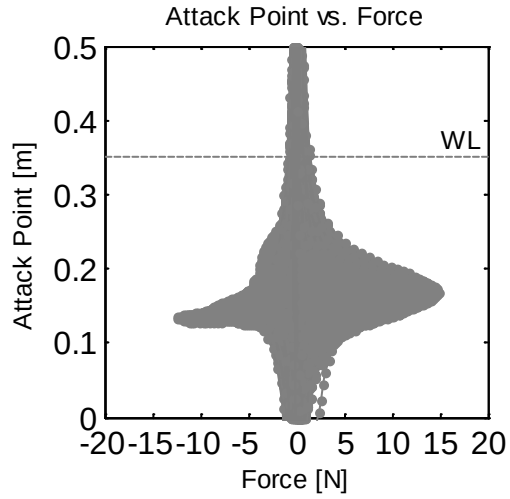
Attack Point vs. Force
Attack Point [m]
Force [N]
WL
0.5
0.4
0.3
0.2
0.1
0
-20 -15 -10 -5 0 5 10 15 20

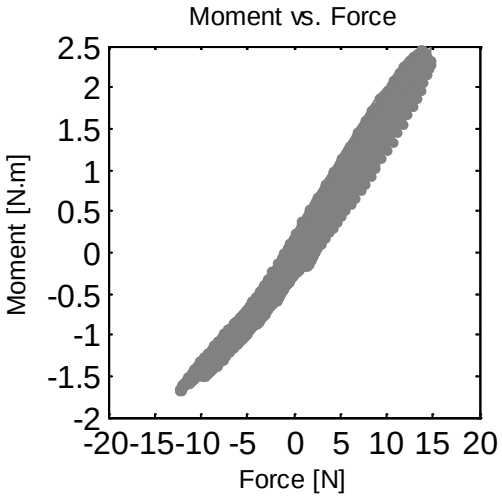
Moment vs. Force
Moment [N.m]
Force [N]
2.5
2
1.5
1
0.5
0
-0.5
-1
-1.5
-2
-20 -15 -10 -5 0 5 10 15 20

(6.1)

(6.2)

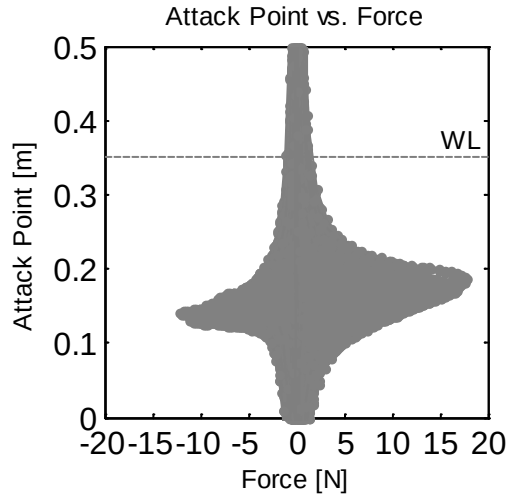
Attack Point vs. Force
Attack Point [m]
Force [N]
WL
0.5
0.4
0.3
0.2
0.1
0
-20 -15 -10 -5 0 5 10 15 20

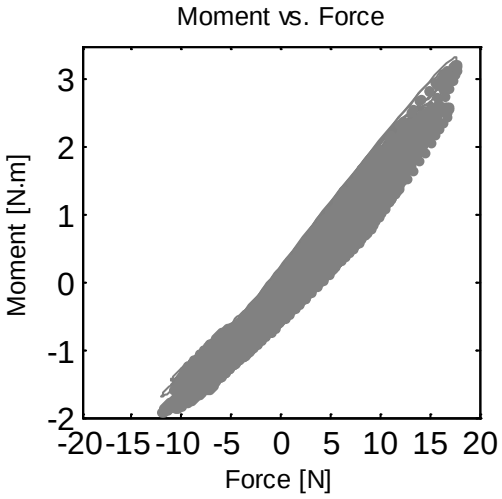
Moment vs. Force
Moment [N.m]
Force [N]
3
2
1
0
-1
-2
-20 -15 -10 -5 0 5 10 15 20

(7.1)

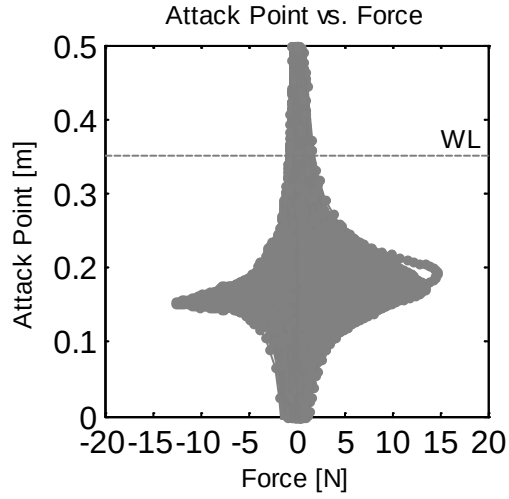
Attack Point vs. Force
Attack Point [m]
Force [N]
WL
0.5
0.4
0.3
0.2
0.1
0
-20 -15 -10 -5 0 5 10 15 20

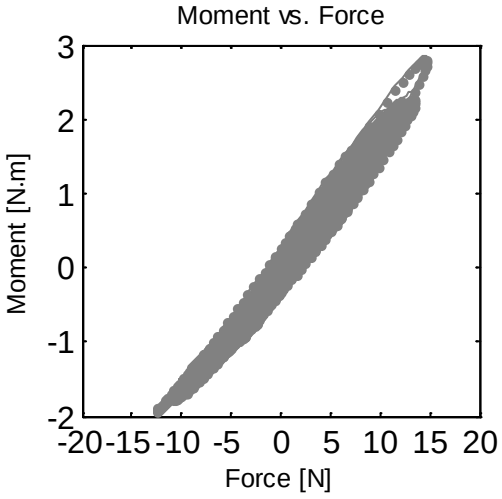
Moment vs. Force
Moment [N.m]
Force [N]
3
2
1
0
-1
-2
-20 -15 -10 -5 0 5 10 15 20

(7.2)

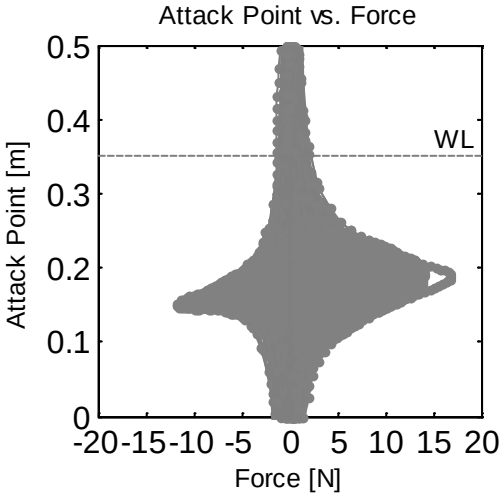
Attack Point vs. Force
Attack Point [m]
Force [N]
WL
0.5
0.4
0.3
0.2
0.1
0
-20 -15 -10 -5 0 5 10 15 20

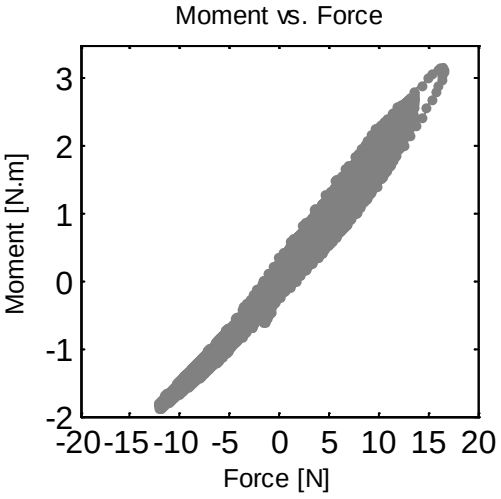
Moment vs. Force
Moment [N.m]
Force [N]
3
2
1
0
-1
-2
-20 -15 -10 -5 0 5 10 15 20

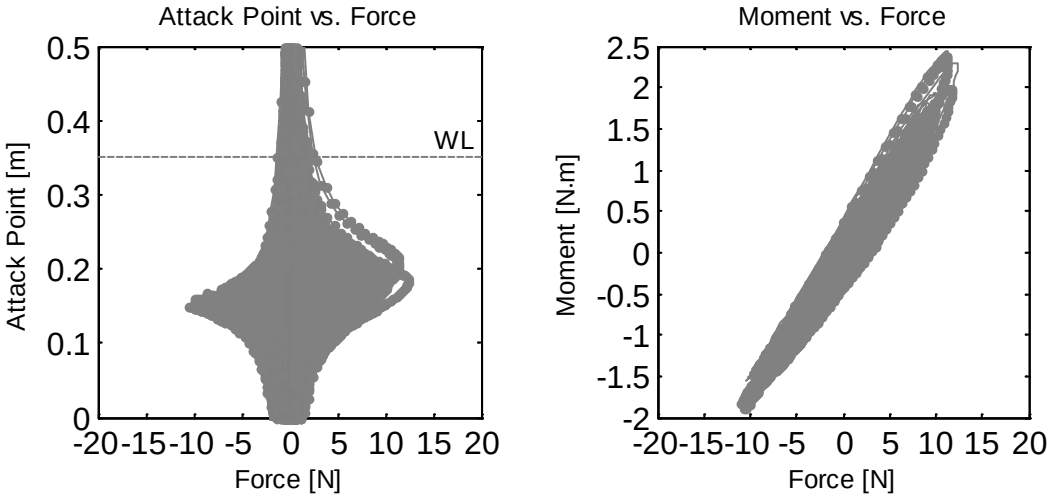

(8.1)

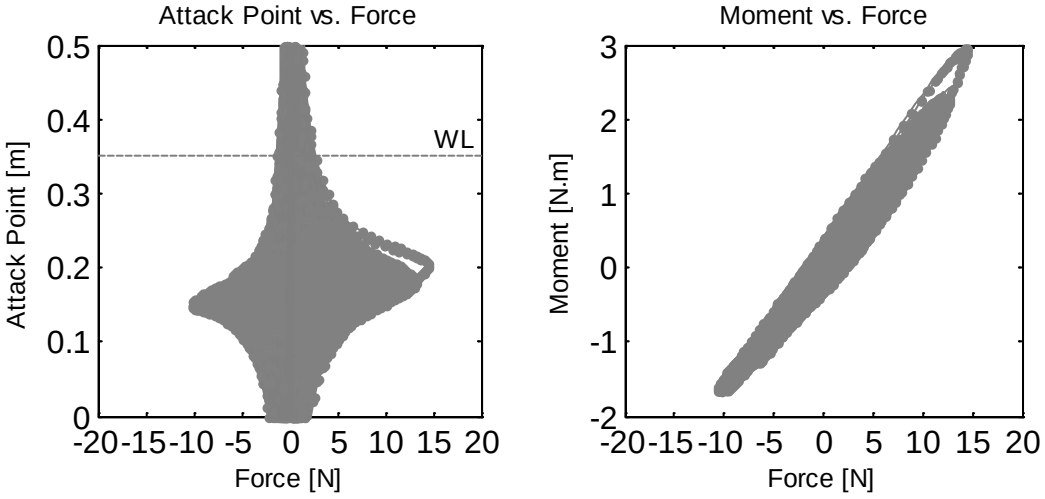

(8.2)

Figure 1: The point of attack as a function of the horizontal force (to the left). Moment as a function of the horizontal force (to the right): 1) assigned H_s = 0.095 m, T_p = 1.4 s (Fig. 1.1-8.1, TP1-TP8); 2) assigned H_s = 0.115 m, T_p = 1.4 s (Fig. 1.2-8.2, TP1-TP8).For the reference case (monopile) the figures are also given for 3 consecutive waves.

NOTATION

B width of the wave flume [m]

C_D drag coefficient

C_M inertia (mass) coefficient

C_A added mass coefficient

D diameter [m]

F maximum wave force (irregular wave conditions) [N]

F_{max} maximum wave force (regular wave conditions) [N]

F_{Hmax} highest maximum wave force [N]

$F_{2\%}$ maximum peak force for the wave height with an exceedance probability of 2% [N]

g acceleration of gravity [m/s^2]

h water depth [m]

H wave height [m]

$H_{2\%}$ wave height with an exceedance probability of 2% [m]

H_s significant wave height [m]

H_{max} maximum wave height [m]

k roughness height [m]

KC Keulegan-Carpenter number

L wavelength [m]

M maximum moment (irregular wave conditions) [N·m]

M_{max} maximum moment (regular wave conditions) [N·m]

$M_{2\%}$ maximum peak moment for the wave height with an exceedance probability of 2% [N·m]

q discharge [m^3/s]

Re Reynolds number

t water temperature of the water in the wave flume [ºC]

T wave period or period of oscillation [s]

T_p peak wave period [s]

U current velocity [m/s]

V total flow velocity [m/s]

V_m maximum orbital particle velocity at the wave crest [m/s]

ν fluid kinematic viscosity [m^2/s]

Δ nondimensional roughness

ρ mass density of water [kg/m^3]

ISSN 1901-7278
DCE Technical Memorandum No. 28